2020

A Review of Vegetation Phenological Metrics Extraction Using Time-Series, Multispectral Satellite Data

Linglin Zeng
Huazhong Agricultural University

Brian D. Wardlow
University of Nebraska-Lincoln, bwardlow2@unl.edu

Daxiang Xiang
Changjiang River Scientific Research Institute, Changjiang River Water Resources Commission

Shun Hu
Wuhan University

Deren Li
Wuhan University

Published in *Remote Sensing of Environment* 237 (2020), 111511; doi: 10.1016/j.rse.2019.111511

Submitted November 30, 2018; revised August 2, 2019; accepted October 28, 2019; published online November 22, 2019.

A Review of Vegetation Phenological Metrics Extraction Using Time-Series, Multispectral Satellite Data

Linglin Zeng,[1] Brian D. Wardlow,[2] Daxiang Xiang,[3] Shun Hu,[4] and Deren Li[5]

1. College of Resources and Environment, Huazhong Agricultural University, Wuhan, China
2. Center for Advanced Land Management Information Technologies, School of Natural Resources, University of Nebraska–Lincoln, Lincoln, Nebraska, USA
3. Changjiang River Scientifc Research Institute, Changjiang River Water Resources Commission, Wuhan, China
4. State Key Laboratory of Water Resources and Hydropower Engineering Sciences, Wuhan University, Wuhan, China
5. State Key Laboratory of Information Engineering in Surveying, Mapping and Remote Sensing, Wuhan University, Wuhan, China

Corresponding author – Brian D. Wardlow, email bwardlow2@unl.edu

Abstract

Vegetation dynamics and phenology play an important role in inter-annual vegetation changes in terrestrial ecosystems and are key indicators of climate-vegetation interactions, land use/land cover changes, and variation in year-to-year vegetation productivity. Satellite remote sensing data have been widely used for vegetation phenology monitoring over large geographic domains using various types of observations and methods over the past several decades. The goal of this paper is to present a detailed review of existing methods for phenology detection and emerging new techniques based on the analysis of time-series, multispectral remote sensing imagery. This paper summarizes the objective and applications of detecting general vegetation phenology stages (e.g., green onset, time or peak greenness, and growing season length) often termed "land surface phenology," as well as more advanced methods that estimate species-specific phenological stages (e.g., silking stage of maize).

Common data-processing methods, such as data smoothing, applied to prepare the time-series remote sensing observations to be applied to phenological detection methods are presented. Specific land surface phenology detection methods as well as species-specific phenology detection methods based on multispectral satellite data are then discussed. The impact of different error sources in the data on remote-sensing based phenology detection are also discussed in detail, as well as ways to reduce these uncertainties and errors. Joint analysis of multiscale observations ranging from satellite to more recent ground-based sensors is helpful for us to understand satellite-based phenology detection mechanism and extent phenology detection to regional scale in the future. Finally, emerging opportunities to further advance remote sensing of phenology is presented that includes observations from Cubesats, near-surface observations such as PhenoCams, and image data fusion techniques to improve the spatial resolution of time-series image data sets needed for phenological characterization.

Keywords: land surface phenology, species-specific phenology, remote sensing, data smoothing, phenological metrics extraction

1. Introduction

The word "phenology" is derived from the Greek word "phaino," which means to show or appear. From a scientific perspective, phenology is defined as the study of recurring plant and animal life cycle stages by Lieth (1974) that is often composed of specific botanical and agronomic plant-growth stages (e.g., bud burst, leaf emergence, and flowering). Traditionally, vegetation phenology refers to specific life cycle events based on visual, ground observations of individual plant changes such as budbreak, leaf out, and leaf senescence of forest and emergence, flowering, and maturity of cereal crops (Verhegghen et al., 2014; de Beurs and Henebry, 2005). The observation of these traditional phenological stages corresponding to specific vegetation physiological processes provide natural resource management. Precision agriculture is a particular area in which crop-specific phenological monitoring plays an important role in farm management decisions such as fertilization, irrigation, and other chemical applications, as well as can serve as an indicator of crop productivity (Sakamoto et al., 2013; Funk and Budde, 2009).

While, from a remote-sensing perspective, many of these specific phenological events cannot be directly detected at the spatial resolutions of satellite imagery and thus more general descriptors of vegetation dynamics termed "land surface phenology" (LSP) are calculated. de Beurs and Henebry (2005) defined LSP as the spatio-temporal development of the vegetated land surface as revealed by spectral observations from satellite sensors. LSP metrics are typically associated with general inter-annual vegetation changes interpretable from spectral remote sensing imagery such as start of greening/season (SOS), the peak of growing season, onset of senescence or end of the season (EOS), and growing season length (Beurs and Henebry, 2010; Reed et al., 1994), as well as other transition stages (e.g., maturity (Zhang et al., 2003)).

Phenological stages can be detected from several types of observations that include: (1) human visual observations, (2) near-surface measurement, and (3) satellite remote sensing. Human visual observations of plant phenology stages have been conducted for more than a century for many locations, and there are major observer networks in several parts

of the world, such as the Pan European Phenology Network (PEPN) (Templ et al., 2018; Vliet et al., 2003) and the National Phenology Network (NPN) (Mayer, 2010) in the United States. Although these efforts are critical and provide detailed plant phenology information at species-scale or individual plant scale (e.g., common lilac, *Syringa vulgaris*), they represented only a small localized area and are often limited in number. Such visual observations provide detailed and accurate phenology information that is vital for calibration and validation of remote sensing–based models for vegetation phenology estimation. Near-surface observations generally include imagery acquired from conventional visible-wavelength digital cameras with typically RGB (Red, Green, and Blue) bands (Wingate et al., 2015; Vrieling et al., 2018; Nijland et al., 2016), continuous carbon flux measurements (Wu et al., 2013), and spectral reflectance sensors with multiband radiometer similar to the sensors carried on the satellites but mounted on tripod, fence post, meteorological tower or carried on aerial platform, e.g. unmanned aerial vehicle (UAV) (Berra et al., 2019). Near-surface measurements such as these can provide higher temporal resolution and greater spatial coverage than visual observations and can be used to analyze site-level phenological variation and mechanisms, train satellite remote sensing–based phenological models, and evaluate the results (Vrieling et al., 2018), bridging the scale between visual observations and satellite-based imagery (Sonnentag et al., 2012).

Specifically, automated digital camera imagery offers economical, objective, and high temporal and spatial resolution observations that have been increasingly used in localized phenology studies (Sonnentag et al., 2012; Julitta et al., 2014; Wingate et al., 2015; Nijland et al., 2016; Vrieling et al., 2018). Unlike the multispectral radiometer carried on satellites, due to the absence of near-infrared channel, digital cameras use the RGB-based vegetation index (VI) (e.g., the green chromatic coordinate (GCC)) to quantify canopy greenness (Klosterman et al., 2014a,b). Digital cameras have been implemented by various networks (Richardson et al., 2011; Klosterman et al., 2014a,b; Moore et al., 2016; Nasahara and Nagai, 2015; Wingate et al., 2015). For example, the PhenoCam network (https://phenocam.sr.unh.edu/webcam/) provides freely accessed digital images from tower-mounted web cameras across a range of ecosystem types at continental scale (Liu et al., 2017b; Sonnentag et al., 2012; Richardson et al., 2011). PhenoCam network was started in 2006 and increasingly used in phenology studies in the last decade (Zhang et al., 2018; Liu et al., 2017b; Klosterman et al., 2014b, 2014a; Hufkens et al., 2012; Richardson et al., 2018).

Visual and near-surface observations (hereinafter both of them refer as ground-based observations (Graham et al., 2010; Sonnentag et al., 2012)) at a site-level scale are usually limited in number and spatial coverage. Satellite-based remote sensing offers global coverage data for large-scale phenological research (Zhang et al., 2006; Brown et al., 2012). Landsat was the first space-borne sensor used to characterize the seasonality of vegetation at regional scales (Thompson and Wehmanen, 1979). The Landsat series of satellite-based sensor, with a nominal 16-day temporal resolution and 30-m spatial resolution and with a data archive extending from the early 1970s to present, has been appropriate for many landscape characterization applications such as land cover classification, change detection and vegetation stress monitoring. However, the use of Landsat imagery LSP applications is limited because many phenological changes occur more rapidly than the 16-day revisit time of Landsat and cloud cover contamination issues of the optical satellite observations

further reduce the number of Landsat images available to adequately detect many phenological events. The Advanced Very High Resolution Radiometer (AVHRR) has been collecting a near-daily global coverage of coarse-to-moderate spatial resolution (1- and 8-km) providing a consistent time-series of temporallycomposited (e.g., bi-weekly or monthly) observations that have been widely applied for LSP studies at regional to global scales for more than 25 years (Moody and Johnson, 2001; Lloyd, 1990; Duchemt al. 1999; Moulin et al., 1997; Heumann et al., 2007; Reed et al., 1994).

Since the early 2000s, the Moderate Resolution Imaging Spectrometer (MODIS) has provide an improved times-series of multispectral observations acquiring a near-daily global coverage of multispectral imagery with a high temporal (near daily) and moderate spatial resolution (250–500 m) with 7 land-related spectral bands for vegetation applications. The MODIS instrument, with higher spatial resolution in two relevant land-related bands (visible red and near infrared), was a marked improvement over AVHRR. As a result, MODIS data have become increasingly used for phenology studies and vegetation monitoring over large geographic regions (Wardlow and Egbert, 2008; Ahl et al., 2006; Fisher and Mustard, 2007; Tan et al., 2011; Zhang et al., 2003). However, the AVHRR sensor with a much longer historical data records (from 1981) than MODIS (from 2001), is well suited for long-term, multi-decadal studies (Vrieling et al., 2013).

Sentinel-2 is a constellation of two satellites that provides free publicly accessible high-resolution optical imagery at 10–60 m resolution at a 5-day interval since the launch of Sentinel-2B in March 2017 and provides continuity for the current SPOT and Landsat missions (Li and Roy, 2017). These two Sentinel-2 satellites with rigorously calibrated sensor systems to some extent overcome the spatiotemporal constraints of current frequently used satellite sensors and show potential in ongoing phenology studies (Vrieling et al., 2018; Jönsson et al., 2018; Jian and Roy, 2017; Zhou et al., 2019). However, the achievable frequency is still suboptimal for phenology studies in the areas with rapid vegetation dynamics or frequent cloud cover (Houborg and Mccabe, 2018). While small satellite constellation (e.g. Planet-Scope) providing daily 3m spatial resolution have been providing unparalleled opportunities for local-to-global scale monitoring (Houborg and Mccabe, 2018; Vrieling et al., 2018; Adole et al., 2016).

Visible Infrared Imaging Radiometer Suite (VIIRS), which was launched in 2011, has been providing a comparable time-series of multispectral image data to AVHRR and MODIS set that is increasingly be applied for vegetation phenology (Liu et al., 2017a; Zhang et al., 2018). VIIRS is intended be a continuity mission to provide a long-term, operational time-series multispectral data need to derived VI data consistent with the VI data record of AVHRR and MODIS, producing an ongoing, inter-sensor time series of VI data spanning from the early 1980s into the future. SPOT-VEGETATION is another multi-spectral global imager that has provided time-series VI data for various vegetation phenological studies (Guyon et al., 2011; Meroni et al., 2013; Yang et al., 2016). The MEdium Resolution Imaging Spectrometer (MERIS) is an additional global imager that has been used to produce the MERIS Terrestrial Chlorophyll Index (MTCI), which is sensitive to chlorophyll changes and has been applied for phenology studies (Boyd et al., 2011; Dash et al., 2010; He et al., 2015). Geostationary satellites with very high temporal resolution (up to 30 s) such as Geostationary Operational Environmental Satellite-R Series (GOES-R), Spinning

Enhanced Visible and Infrared Imager (SEVIRI), and Himawari-8 also offer promising new data sources for phenology studies in low latitude areas and other cloud-prone regions with frequent cloud cover and few cloud-free observations available from even daily retrieved sensors such as MODIS during the key phenological stages (Guan et al., 2014; Yan et al., 2016a).In addition to multispectral-based VIs, several other remote sensing–derived variables including vgetation optical depth (VOD) retrievals derived from microwave sensors (Jones et al., 2011), solar-induced chlorophyll fluorescence (SIF) (Jeong et al., 2017) and Synthetic Aperture Radar (SAR) polarimetric parameters (McNairn et al., 2018) were also used for phenology studies.

Since the 1980s, vegetation phenology studies have provided a basis for monitoring inter-annual variations and long-term trends in vegetated land surface characteristic, classifying land cover types based on their multitemporal seasonal spectral response (Badhwar, 1984; Townshend et al., 1991; de Beurs and Henebry, 2004), analyzing the connections interactions between vegetation phenology dynamics and climate variables such as precipitation and temperature (Shen et al., 2011; Tateishi and Ebata, 2004), measuring the responses of vegetation to climate change (Heumann et al., 2007; Yu et al., 2003), assessing intra- and interannual fluctuations in the terrestrial carbon balance (Han et al., 2018; Keenan et al., 2014; Garrity et al., 2011) and anthropogenic activities over the landscape (Li et al., 2017). In addition, the temporal and spatial variability of vegetation phenology variations help distinguish different vegetation types (Xue et al., 2014; Wang et al., 2013), especially crops (Wardlow and Egbert, 2008) and drought-related plant stress conditions(Brown et al., 2008; Meroni et al., 2013) from a delayed growing season vegetation response due to other climatic conditions (e.g., late freeze or excessive moisture).

This paper presents a detailed overview of historical remote sensing–based LSP methods and more recent developments of crop vegetation phenology detection base on time-series satellite imagery. The impacts of different error sources in the remotely sensed spectral image data are discussed in detail followed by the analysis on how to reduce the different errors for vegetation phenology detection. Finally, the challenges and opportunities for satellite-derived phenology are discussed. The estimation of phenological metrics from times-series remote sensing data generally consist of three key steps: (1) data cleaning and flagging; (2) data smoothing and time-series data reconstruction, and (3) phenological metrics extraction based on the reconstructed time series data. Many methods have been proposed in previous studies for the subsequent data smoothing and time-series data reconstruction and phenological estimate steps, which will be summarized in depth in sections 2, 3, and 4, respectively.

2. Vegetation indices and data smoothing methods

Traditionally, that analysis of remote sensing-based VI data transformed from individual spectral bands has been the basis for most LSP studies rather than directly using data from the spectral bands. The use of VIs is well established in the literature because the represent spectral transformations that integrate two or more spectral bands sensitive to different plant characteristics (e.g., pigments, water content, or structure) and have been found to be more useful indicators of the state and condition of vegetation than the analysis of data from individual bands (Wagenseil and Samimi, 2006b; Galford et al., 2008; Hall-Beyer,

2003; Vrieling et al., 2018). Historically, the normalized difference vegetation index (NDVI) (Rouse, 1973) data has been widely used for phenology characterization (Fischer, 1994; Moody and Johnson, 2001; Balzter et al., 2007; Yu et al., 2003) because it is simple to calculate using the visible red (sensitive to chlorophyll pigment content) and near-infrared (sensitive to internal leaf structure) spectral bands that are commonly part of most optical sensors. With the launch of more recent sensors such as MODIS and MERIS, the number of land-related bands has expanded to include other spectral regions (e.g., visible green and middle infrared) allowing a number of new VIs to be calculated that are designed to detect specific plant characteristics (e.g., chlorophyll content, leaf area, and plant water content) (Table 1).

Table 1. Summary of common satellite-derived remote sensing indices used in phenology studies

Class	Index	Calculation	Characteristic	Reference
Ratio and combined Index	NDVI	$\frac{\rho NIR - \rho Red}{\rho NIR + \rho Red}$	Sensitive to chlorophyll, but saturated to flourish vegetation	Rouse (1973)
	WDRVI	$\frac{\alpha \times \rho NIR - \rho Red}{\alpha \times \rho NIR + \rho Red}$	Similar to NDVI, but still sensitive to flourish vegetation	Gitelson (2004)
	NDWI	$\frac{\rho NIR - \rho SWIR}{\rho NIR + \rho SWIR}$	Sensitive to the water	Gao (1996)
	GRVI	$\frac{\rho Green - \rho Red}{\rho Green + \rho Red}$	Sensitive to land cover types	Tucker (1979)
	MTCI	$\frac{\rho 735.75 - \rho 708.75}{\rho 708.75 + \rho 681.25}$	Sensitive to high chlorophyll content and limited sensitive to atmospheric effect or spatial resolution	Dash and Curran (2004)
	PI	$PI = \begin{Bmatrix} 0, if\ NDVI\ or\ NDWI < 0 \\ NDVI^2 - NDWI^2 \\ 0, if\ PI = 0 \end{Bmatrix}$	Designed to remove the wetness (e.g., snow) and brighten effect (e.g., soil) on greenness	Gonsamo et al. (2012)
	PPI	$PPI = -K \times \ln\left(\frac{M - DVI}{M - DVIs}\right)$ $DVI = \rho NIR - \rho Red$	Derived from radiative transfer theory	Jin and Eklundh (2014)
	NDPI	$\frac{\rho NIR - (\alpha \times \rho Red + (1-\alpha) \times \rho SWIR)}{\rho NIR + (\alpha \times \rho Red + (1-\alpha) \times \rho SWIR)}$	To contrast vegetation from the background and to minimize the difference among the backgrounds	Cao et al. (2018)
Physically based index	LAI	By model fitting (e.g., linear model, piecewise logistic model)	Important structural parameter, but unable to be derived directly from satellite imagery	Watson (1947)

Table 1. *Continued*

Class	Index	Calculation	Characteristic	Reference
	fAPAR	Several algorithms have been developed, e.g., JRC, MODIS algorithm	Based on definite physiological significance, but unable to be derived directly from satellite imagery	(Myneni, 2003; Gobron et al., 2006)
Adjusted VI	EVI	$\frac{\rho NIR - \rho Red}{\rho NIR + C1 \times \rho Red - C2 \times \rho Blue + L}$	Introducing atmosphere-sensitive blue band to correct the red band for aerosol influences	Huete et al. (1999)
	EVI2	$G\frac{\rho NIR - \rho Red}{\rho NIR + (6 - 7.5/c)\rho Red + 1}$	Similar to EVI, retaining the soil-noise adjustment function and maintaining the improved sensitivity and linearity in high biomass regions, with the absence of a blue band	Jiang et al. (2008)
	PVI	$\frac{\rho NIR - a1 \times \rho Red - a2}{\sqrt{1 + a_1^2}}$	Designed to minimize its sensitivity to soil reflectance	Richardson and Wiegand (1978)
	SAVI	$\frac{(\rho NIR - \rho Red)(1 + N)}{\rho NIR - \rho Red + N}$	Designed to minimize soil brightness influences	Huete (1988)

Where ρ_{Red}, ρ_{Green}, ρ_{NIR}, and ρ_{SWIR} are reflectance in red, green, near-infrared and short-wave infrared band, respectively. DVIS is the DVI of the soil estimated from soil spectral reflectance. K is a gain factor. $\rho_{681.25}$, $\rho_{708.75}$, and $\rho_{753.75}$ are reflectance of band 8, 9 and 10 in the MERIS band setting. α is the weighting coefficient. G is determined by C value, and C is derived by linear fitting ($\rho_{Red} = c \times \rho_{NIR}$). a_1 and a_2 are soil parameters related to NIR reflectance and RED reflectance over nonvegetated surfaces. L is the vegetation background adjustment. Factor N is a constant.

The most commonly used remote sensing VIs used in phenology literature include the NDVI (Wagenseil and Samimi, 2006a; Hogda et al., 2001; Kariyeva and Leeuwen, 2011; Wu et al., 2017; Pan et al., 2015; Hou et al., 2014), enhanced vegetation index (EVI) (Cao et al., 2015; Verhegghen et al., 2014; Zhang et al., 2003; Wang et al., 2017), leaf area index (LAI) (Kang et al., 2003; Hanes and Schwartz, 2011; Wang et al., 2017), wide dynamic range vegetation index (WDRVI) (Sakamoto et al., 2010; Wu et al., 2014), as well as other less frequently used indices like MERIS Terrestrial Chlorophyll Index (MTCI) (Boyd et al., 2011; Dash et al., 2010; He et al., 2015), fraction of absorbed photosynthetically active radiation (fAPAR) (Verstraete et al., 2008; Meroni et al., 2014), perpendicular vegetation index (PVI) (Guyon et al., 2011), green-red vegetation index (GRVI) (Motohka et al., 2010), two-band enhanced vegetation index (EVI2) (Yan et al., 2016a; Yan et al., 2016b; Jiang et al., 2008), plant phenology index (PPI) (Jin et al., 2017), and soil-adjusted vegetation index (SAVI) (Wu et al., 2014). An index such as the WDRVI makes use of the same spectral bands (red and NIR) as NDVI but overcomes the limitation of NDVI becoming saturated and insensitive to changes of high biomass conditions (Gitelson, 2004; Zeng et al., 2016; Sakamoto et al., 2010). Physical-based indices like fAPAR and LAI represent direct biophysical

measures of vegetation, can be estimated by empirical or physical models, instead of a certain combination (formula) of the multispectral reflectance properties (Myneni, 2003; Gobron et al., 2006). The modified VIs such as PVI, SAVI, EVI, and EVI2 are designed to minimize the index's sensitivity to various environmental factors that introduce non-vegetation-related variations into NDVI that include effects from the soil background, snow or aerosols (Yu et al., 2003; Guyon et al., 2011; Wu et al., 2014). In addition, several studies suggest that a collectively analysis of multiple VIs may improve the accuracy of phenology estimation (Walker et al., 2014; Wu et al., 2014; Gonsamo et al., 2012).

To reduce noise such as cloud contamination, off-nadir viewing effects, sun-angle, shadow effects and other data errors, empirical method: maximum value composite (MVC) method is commonly applied to the satellite-derived observations to generate temporally composite data (e.g., widely used MODIS 8- and 16-day composite products), before other data smoothing methods applied. Most of the phenological studies that used the satellite data with high temporal resolution are based on these composite products (Jönsson and Eklundh, 2002; Zeng et al., 2016; Zhang et al., 2006; Sakamoto et al., 2005). MVC method typically selects the highest VI value from a series of daily VI images for a defined temporal composting window (e.g., 8 days or 1 month) to represent the land surface conditions for that time periods in the time series data set (Holben, 1986), as it is assumed that the atmospheric conditions and other types of noise artificially lowers the NDVI values. It is a simple and effective method to reduce noise and establish a representative time series of land surface conditions. However, in some cases, the MVC method cannot always find a noise-free value during prolonged cloudy periods, which can result in a less than optimal VI value to represent the composite time interval. One strategy to address this issue is to increase the temporal compositing period, but this comes at the cost of potentially losing phenology information as key phenological events may occur during a shorter time period and not be detected within this longer compositing interval.

The time-series VI data set generated during the initial, temporal compositing step still included various noise components (Hird and Mcdermid, 2009; Jönsson and Eklundh, 2004; Zhang et al., 2003; Atkinson et al., 2012). Smoothing methods are typically applied to the time-series VI data set to minimize this residual noise and reconstruct a more representative data time series vegetation condition. Several smoothing options are available and the specific method selected can influence the performance of the phenology extraction from the smoothed time series (Kandasamy et al., 2013; Atkinson et al., 2012; Hird and Mcdermid, 2009). The techniques used to smooth and reconstruct the time-series data can be classified into 3 categories (Table 2) (Atkinson et al., 2012): (1) an empirical methods, (2) curve-fitting methods, and (3) data transformations. Details of these categories of smoothing methods are presented in the following subsections.

Table 2. Summary of common data smoothing methods

	Description	Classification	Processing window	Reference
Maximum value compositing (MVC)	Selecting the highest value to represent the condition for a certain period	Empirical Method	Local	Holben (1986)
Locally weighted regression	Estimating a regression surface by fitting a function of the independent variables locally	Filtering Method	Local	Cleveland and Devlin (1988)
Best Index Slope Extraction (BISE)	The decrease only accepted if there is no point in a sliding period with a value greater than a certain threshold	Empirical Method	Local	(Viovy et al., 1992; Lovell and Graetz, 2001)
Fast Fourier transform	Using a least squares method to fit the first three harmonics	Data transformation	Whole	Sellers et al. (1994)
Empirical mode decomposition	Decomposition into IMFs by "sifting"	Data transformation	Whole	Huang et al. (1998)
Temporal Window Operation (TWO)	Apply linear interpolation to remove low NDVI value within a defined temporal window	Empirical Method	Local	(Park et al., 1999)
Harmonic ANalysis of Time Series (HANT)	Decomposes into a series of trigonometric functions	Data transformation	Whole	Roerink et al. (2000)
Discrete Fourier Transform (DFT)	Decompose the temporal data to the frequency domain	Data transformation	Whole	Moody and Johnson (2001)
Asymmetrical Gaussian (AG) function-fitting	Fitting to AG Functions	Curve fitting	Local	Jönsson and Eklundh (2002)
Logistic function-fitting	Fitting to Logistic function with different options parameters	Curve fitting	Local	(Beck et al., 2006; Fisher et al., 2006; Zhang et al., 2003; Elmore et al., 2012; Cao et al., 2015; Zhang, 2015)
Whitaker	Fitted by penalized least square regression	Curve fitting	Whole	Eilers (2003)
Savitzky-Golay filter	Savitzky-Golay filter with iterations to the upper envelope or flexible window	Curve fitting	Local	(Chen et al., 2004; Verger et al., 2011)
Quadratic function-fitting	Simple regression models describing NDVI as a quadratic function of accumulated growing degree-days	Curve fitting	Local	de Beurs and Henebry (2004)
Wavelet-based Filter	Decomposed to linear combinations of wavelet functions	Data transformation	Whole	Sakamoto et al. (2005)
Mean-value iteration filter	Iteratively compares and replaces with average value if it is above a certain threshold	Empirical Method	Local	Ma and Veroustraete (2006)
Locally adjusted cubic-spline	Determine local smoothing parameter by the local curvature of time series	Curve fitting	Local	Chen et al. (2006)
Non-classical high order Fourier Transform	Applying high-order Fourier with roughness damping	Data transformation	Whole	Hermance (2007)
High-Order Annual Splines	Applying annual high-order polynomial splines with roughness damping	Curve fitting	Local	Hermance et al. (2007)

Table 2. *Continued*

	Description	Classification	Processing window	Reference
Iterative Interpolation	Iteratively compares to an average of different years and replaces with average value	Empirical Method	Local	Julien and Sobrino (2010)
Changing-weight filter method	Apply a three-point changing-weight filter based on local minimum/maximum points in time series	Empirical Method	Local	Zhu et al. (2012)
Compound smoother RMMEH	Include several operations, such as running weighted moving average, maximum operation, arithmetic average, medians smoother	Empirical Method	Local	Jin and Xu (2013)
Parametric Double Hyperbolic Tangent model	Apply a seven-parameters hyperbolic tangent model to fit the asymmetric timeseries curves	Curve fitting	Local	Meroni et al. (2014)
Spatial-temporal Savitzky-Golay (STSG)	Employs both neighboring pixels and multi-year data for noise reduction	Curve fitting	Local	Cao et al. (2018)
Shape-Prior–based method	Based on box constrained separable least squares fits combined with seasonal shape priors	Curve fitting	Local	Jönsson et al. (2018)

Labels: "Whole" and "local" denoting their flexibility to generalize across the full growing season, respectively, or to match details in the time-series (Cai et al., 2017).

2.1. Empirical methods

Empirical smoothing methods operate over a local temporal window within the time series based on empirical knowledge or assumptions. For example, it is generally assumed that noise signals usually reduce the VI value and temporal variation of the VI signal from vegetation should be a smooth, continuous response across the growing season under favorable conditions (i.e., a steady, continuous VI increase during the green up phase followed by a continuous decrease during the senescence phase). Based on this assumption, several empirical approaches such as running sliding window (Viovy et al., 1992), moving average filter (Ma and Veroustraete, 2006), iterative interpolation (Julien and Sobrino, 2010), changing-weight filter (Zhu et al., 2012), compound smoother (Jin and Xu, 2013), etc., were proposed to replace the low VI values caused by residual noise.

The advantage of these traditional empirical methods is that they are simple to apply, but they are usually sensitive to the empirical parameters such as the threshold for noise, the length of compositing period for the MVC method and the length of sliding window. Specifically, they performed poorly when the original time series contains continuous missing data (Jönsson et al., 2018; Cao et al., 2018). Recently, the methods integrating spatial and/or temporal information were proposed to reconstruct VI time-series data (Jönsson et al., 2018; Cao et al., 2018; Julien and Sobrino, 2010). The VI values of neighboring pixels (Cao et al., 2018) and composited historical clear-sky VI values (Julien and Sobrino, 2010; Jönsson et al., 2018) have proven helpful to reconstruct the time-series data at the pixel level, especially for periods of continuous missing data.

Only applying traditional empirical methods to create a smoothed time series representative of detailed phenological responses can still retain some residual noise artifacts in the form of localized, anomalous peaks or dips in the time-series VI data. Accordingly,

other data smoothing methods like curve fitting and data transformation can be used after the application of empirical methods to further reduce these remaining noise artifacts.

2.2. Curve fitting method

Curve fitting methods apply mathematical functions to fit the VI time-series curves to a specified function. Widely used approaches include logistic models (Zhang et al., 2003), improved logistic method (Elmore et al., 2012; Cao et al., 2015; Beck et al., 2006; Fisher et al., 2006), asymmetric Gaussian functions (Jönsson and Eklundh, 2002, 2004), Savitzky–Golay (Chen et al., 2004), quadratic function (de Beurs and Henebry, 2004), and nonlinear spherical model (de Beurs and Henebry, 2005). Curve fitting is the most common phenology detection method. For example, Zhang et al., (2003) logistic method was adapted by MODIS Global Land Cover Dynamics Product (MLCD). The asymmetric Gaussian method developed by Jönsson and Eklundh (2002) was applied for temporally smoothing data and estimating phenological metrics for NACP (North American Carbon Program) (Tan et al., 2011).

The model fitting methods can effectively suppress the noise of data. In addition, they are expected to be more objective approaches and easier to adapt to a wide range of situations, as mathematical functions are used to approximate the time-series trajectory of vegetation growth and no predefined thresholds or empirical constraints need to be applied. However, the time series VI curves derived from remote sensing data are not always regular curves (e.g., not sinusoidal or strictly periodic), and the accuracy of function fitting will directly affect the precision and accuracy of extracting some phenological features. An inadequately calibrated data record can introduce artifactual changes in the time series data (de Beurs and Henebry, 2004) and an overfitting of the time series may dampen important phenological features. For example, the greenness trajectory during the senescence phase of the growing season can drop more rapidly than the rapid VI value increase during the spring green-up phase for most vegetation types, or even appear as a two-stage decline (before a more rapid drop-off in autumn, there might be several months of gradually decreasing greenness), which results in estimates of EOS in autumn often being inherently more uncertain (Ganguly et al., 2010; Guyon et al., 2011; Elmore et al., 2012).

To account for more complex time-series VI curves, additional parameters are often defined for improved curve fitting functions. For example, Beck et al. (2006) and Fisher et al. (2006) proposed a double logistic function that fit parameters controlling slope and phase for both green-up and senescence stages with 6 parameters totally (eq. 2). Compared to the logical model with 4 parameters, 2 additional parameters were added: the phase and slope for senescence. These two parameters can adjust the shape of the sigmoid growth curves for greenup and senescence stages, respectively (Fig. 1a). However, it is not capable of fully capturing the vegetation dynamics when it appears a two-stage decline (Fig. 1b). So, Elmore et al. (2012) used 7 parameters (eq. 3) (added a sloped line to join the spring increasing curve and autumn decreasing curve) for a logistic function that was fitted to the time series VI that could describe the two-stage decline in more detail (Fig. 1b). Zhang (2015) proposed a Hybrid Piecewise Logistic Model (HPLM) algorithm (eq. 4) by adding a vegetation stress factor with biophysical meaning to Elmore et al.'s (2012) model. The model with vegetation stress factor and that without stress factors were compared in fitting

the EVI2 time series with good quality, and the model with better fit was chosen. Compare to Elmore et al.'s (2012) model, HPLM is more flexible and expected to have a better fitting in unfavorable growth condition. In addition, Cao et al. (2015) developed an adaptive local iterative logistic fitting method (ALILF) to analyze the "local range" in the MODIS EVI profile, which allowed specific phenological dates to be more accurately estimated from both EVI profiles with a well-defined S-shaped time series and others that were non-logistic in form.

$$y(t,m) = \begin{cases} \frac{m3}{1+e^{m1-m2t}} + m4 \;\; growth\ stage \\ \frac{m7+St}{1+e^{m5-m6t}} + m8 \;\; senescence\ stage \end{cases} \quad (1)$$

$$y(t,m) = m1 + m2\left(\frac{1}{1+e^{m3-m4t}} + \frac{1}{1+e^{m5-m6t}}\right) \quad (2)$$

$$y(t,m) = m1 + (m2 - m7t)\left(\frac{1}{1+e^{m3-m4t}} + \frac{1}{1+e^{m5-m6t}}\right) \quad (3)$$

$$y(t,m) = \begin{cases} \frac{m3}{1+e^{m1-m2t}} + m4 \;\; Favorable\ growth\ condition \\ \frac{m7+St}{1+e^{m5-m6t}} + m8 \;\; Vegetation\ stress\ condition \end{cases} \quad (4)$$

where y(t,m) is the modeled VI at time t (in DOY), and m (m1, m2, . . . , m7) are the fitting parameters. S is the vegetation stress factor.

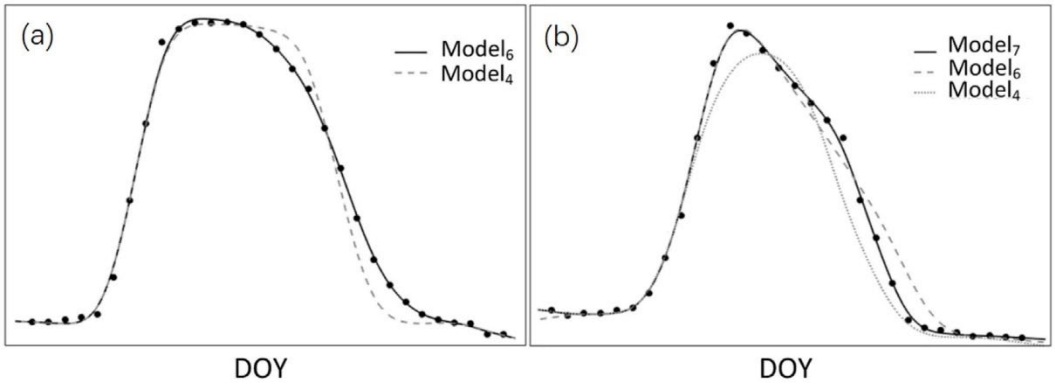

Figure 1. Fit of double logistic functions with 4, 6, and 7 parameters to (a) an asymmetric VI time series and (b) an asymmetric VI time series with a two-stage decline.

2.3. Data transformation methods

Data transformation methods decompose the time series into cyclical, trend, seasonal and irregular (e.g., noise) components based on mathematical manipulation (Zhang and Qi, 2005). Fourier transforms (Moody and Johnson, 2001; Hermance, 2007) and wavelet analysis (Galford et al., 2008; Sakamoto et al., 2005) were the most widely used data transformation methods to characterize the phenology of vegetation from satellite observations.

The classical Fourier methods (e.g., DFT (Moody and Johnson, 2001)), which employ symmetric trigonometric functions (e.g. sine and cosine functions), usually use low-order terms, as high-order terms are apt to retain the noise when capturing shorter period fluctuations, and thus contribute to poor performance of smoothing irregular or asymmetric time series. Hermance (2007) proposed a high-order, nonclassical Fourier method that uses a combination of trigonometric functions and other functions (e.g. polynomial forms and power series). It applied high-order Fourier without concomitant of the spurious oscillations problem for high-order harmonic series through "roughness damping" and improved the resolution of the model (see Hermance, 2007). Generally, the model with higher resolution can better capture subtle phenological information, (e.g. asymmetric logistic functions and double logistic method with more parameters discussed above), as they are able to describe more detailed changes of time-series curves (Jönsson and Eklundh, 2002; Hird and Mcdermid, 2009; Hermance, 2007; Beck et al., 2006). Accordingly, compared to Fourier analysis, wavelet transform based on local basis of functions has advantage in the feasibility of localization in the time domain and flexible scales in both frequency and time domains, which can capture the high frequency variability (e.g. abrupt changes) (Martínez and Gilabert, 2009; Sakamoto et al., 2005).

3. Phenological metrics extraction methods

3.1. LSP detection

Until now, a variety of methods were proposed to extract various LSP metrics (Table 3), which can be classified into two general categories: (1) threshold-based methods and (2) VI change detection methods. The following sections describe the most commonly methods that have been applied in past LSP research.

Table 3. Summary of representative phenological metrics extraction studies using satellite-derived time-series VI data in chronological order in the published literature

Descriptions	Sensors	Data smoothing	Phenology extraction	Detected growth stages	Timeliness	Reference
Fixed VI threshold	AVHRR	Empirical	Threshold	Both vegetation and reproduction stages	Historical detection and real-time monitoring	Lloyd, 1990
Double logistic function fitting with fixed NDVI threshold	AVHRR	Curve fitting	Threshold	Both vegetation and reproduction stages	Historical detection	Fischer, 1994
The intersection of actual time series and the moving average time series	AVHRR	Empirical method	Moving average	Both vegetation and reproduction stages	Historical detection	Reed et al., 1994
Time derivative	AVHRR	Empirical method	Derivative	Both vegetation and reproduction stages	Historical detection	Moulin et al., 1997
Six thresholds of NDVI from 0.1–0.35 in 0.05 increments	AVHRR	Empirical method	Threshold	Both vegetation and reproduction stages	Historical detection and real-time monitoring	Myneni et al., 1997
The average of the gap between maximum and minimum NDVI threshold	AVHRR, MODIS	Curve fitting	Threshold	Both vegetation and reproduction stages	Historical detection	White et al., 1997
Dynamic thresholds based on long-term mean NDVI	AVHRR	Empirical method	Threshold	Both vegetation and reproduction stages	Historical detection and real-time monitoring	Hogda et al., 2001

Table 3. *Continued*

Descriptions	Sensors	Data smoothing	Phenology extraction	Detected growth stages	Timeliness	Reference
Fourier transform and harmonic analysis	AVHRR	Data transformation	Parameter analysis	Both vegetation and reproduction stages	Historical detection	Moody and Johnson, 2001; Hermance, 2007
Locally fit Gaussian functions	AVHRR	Curve fitting	Threshold	Both vegetation and reproduction stages	Historical detection	Jönsson and Eklundh, 2002; Heumann et al., 2007
Maximum change in the NDVI slope angle	AVHRR	Empirical method	Derivative	Both vegetation and reproduction stages	Historical detection	Yu et al., 2003
0.1, 0.2, 0.3 of the gap between maximum and minimum LAI threshold	MODIS	Empirical method	Threshold	Both vegetation and reproduction stages	Historical detection	Kang et al., 2003
Largest derivative	AVHRR	Empirical method	Derivative	Both vegetation and reproduction stages	Historical detection	Tateishi and Ebata, 2004
Two phenometrics extracted based on the fitted convex quadratic model of accumulated growing degree-days	MODIS	Curve fitting	Maximum VI value	Peak season	Historical detection	Henebry and Beurs, 2013; de Beurs and Henebry, 2004
Fitted logistic model with EVI time series and derivative exhibits local minima or maximums	MODIS	Curve fitting	Derivative	Both vegetation and reproduction stages	Historical detection	Zhang et al., 2003a; Beck et al., 2006
TIMESAT software (Savitzky-Golay, double logistic, and asymmetric Gaussian functions) and customizable dynamic threshold (derivative for the improved method)	AVHRR	Curve fitting	Threshold	Both vegetation and reproduction stages	Historical detection	Jönsson and Eklundh, 2004; Tan et al., 2011
NDWI dynamic threshold	SPOT	Empirical method	Threshold	Both vegetation and reproduction stages	Historical detection and real-time monitoring	Delbart et al., 2005a,b
Joint analysis of multi-year Landsat data to build composite VI time-series	Landsat	Curve fitting	Threshold	Both vegetation and reproduction stages	Historical detection and real-time monitoring	Fisher et al., 2006; Melaas et al., 2013
Derivative of local moving window regression	AVHRR	Empirical method	Derivative	Both vegetation and reproduction stages	Historical detection	Balzter et al., 2007
Fourier transformation and inflection point method based on Chlorophyll Index	MERIS	Data transformation	Derivative	Both vegetation and reproduction stages	Historical detection	Dash et al., 2010
Threshold based on temporally normalized brownness index linked with the fraction of fallen leaves and colored foliage	MODIS	Curve fitting	Threshold	Foliage coloration	Historical detection, real-time monitoring, and forecasting	Zhang and Goldberg, 2011
Map vegetation phenology at 30 m resolution using fused MODIS and Landsat data	MODIS and Landsat	Curve fitting	Threshold/ Derivative	Both vegetation and reproduction stages	Historical detection	Walker et al., 2012; Gao et al., 2017
Linear regression by seasonal mean VIs, LST	MODIS	Empirical method	Linear regression	Both vegetation and reproduction stages	Historical detection	Wu et al., 2014
The inflection points from the cumulative NDVI	SPOT	Curve fitting	Derivative	Both vegetation and reproduction stages	Historical detection	Hou et al., 2014; Wu et al., 2016
Adopts an adaptive temporal window and an iterative procedure to fit time series	MODIS	Curve fitting	Local	Vegetation stage	Historical detection	Cao et al. 2015

Table 3. *Continued*

Descriptions	Sensors	Data smoothing	Phenology extraction	Detected growth stages	Timeliness	Reference
Extract phenological dates from single-season high-resolution satellite data by empirically intercalibration of comparable sensors	SPOT5 and RapidEye	Curve fitting	Threshold	Both vegetation and reproduction stages	Historical detection	Vrieling et al. 2017
Apply double hyperbolic tangent model to fit the VI curve and thresholds to estimate start-, peak-, and end-of-season, using Sentinel 2 data of two overlapping orbits	Sentinel 2	Curve fitting	Threshold	Both vegetation and reproduction stages	Historical detection	Vrieling et al., 2018
Proposed a phenology detection method for data-sparse region, which combine seasonal shape priors and box constrained separable least squares fits using Landsat, Sentinel 2, or MODIS only	Landsat, Sentinel 2, and MODIS	Empirical method	Derivative	Both vegetation and reproduction stages	Historical detection	Jönsson et al. 2018
Apply a regression tree modeling framework to estimate phenological metrics using harmonized Landsat-Sentinel-2 data	Landsat and Sentinel 2	Decision tree model	Regression tree model	Both vegetation and reproduction stages	Historical detection and real-time monitoring	Pastick et al., 2018
Complex network-based phenology model	MODIS	Empirical method	Network model	Foliage coloration	Historical detection	Diao, 2019

3.1.1. Threshold-based method

Thresholds methods represent the simplest approach to extract phenological metrics from VI time-series, assuming that the phenological stage commences when the smoothed VI values reach a specific index value (Fig. 2). There are two types of thresholds commonly implemented. One is the "fixed" threshold that arbitrarily establishes a single, fixed index value, like NDVI value reaching 0.17 represents the SOS (Lloyd, 1990; Myneni et al., 1997). The other is the "dynamic" threshold, which is generally based on a metric calculated from the VI time-series data, such as the VI ratio, long-term mean, or median VI of the time-series data record (Hogda et al., 2001; Delbart et al. (2005a,b); White et al., 1997). For example, White et al. (1997) determined the SOS and EOS threshold as the 50% of the VI amplitude. Shabanov et al. (2002) used the NDVI values on DOY 120 and 270 of the baseline year as the SOS and the EOS thresholds by comparing time series of years among each other over the specified area the phenology metrics would be calculated (Shabanov et al., 2002).

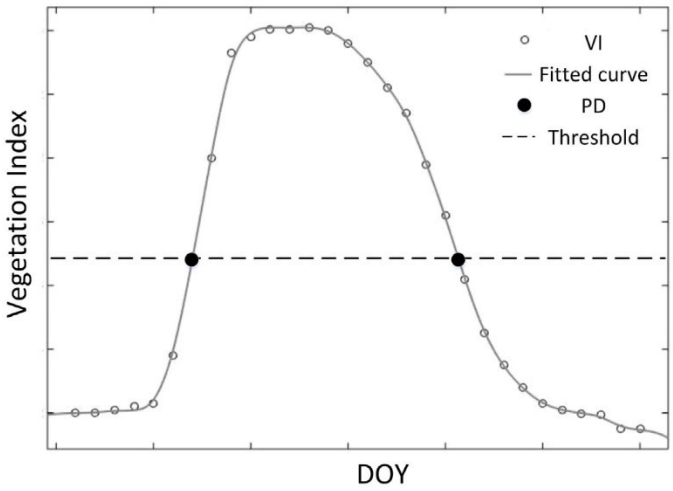

Figure 2. A schematic showing how phenological dates (PD) are extracted by threshold method. The PD can be extracted as the timing when VI values reach the predefined fixed or dynamic threshold.

Various VIs and vegetation indicators calculated from satellite observations have been used for the threshold, including NDVI (Fischer, 1994; White et al., 1997; Hogda et al., 2001), NDWI (Delbart et al. (2005a,b)), EVI (White et al., 2014), temporally normalized brownness index (Zhang and Goldberg, 2011), LAI (Kang et al., 2003), and GRVI (Motohka et al., 2010). For example, Kang et al. (2003) applied dynamic thresholds based on LAI values to detect the SOS in temperate mixed forests of Korea. Zhang and Goldberg (2011) propose a temporally normalized brownness index to represents relative changes in colored foliage and applied thresholds to determine six fall foliage coloration phases.

The NDVI is the widely used VI in threshold methods, but it is not the optimal index for detecting SOS and EOS in areas where extensive snow cover might be expected because an increase/decrease of NDVI in the SOS/EOS might be due to snowmelt/snow-accumulation instead of actual earlier vegetation onset or leaf senescence (Delbart et al. (2005a,b); Kobayashi et al., 2016). Several approaches have been developed to disentangle remotely sensed phenology and snow seasonality, e.g., combining NDVI with NDWI (Delbart et al. (2005a,b); Gonsamo, 2016), or with temperature data (Liu et al., 2016) or with snow information (Beck et al., 2007), exploring new data like sun-induced chlorophyll fluorescence (Walther et al., 2015) and new phenology index like PPI proposed by Jin and Eklundh (2014).

Although the threshold method is simple and easy to apply, there is no underlying biophysical meaning for the threshold selected and a single threshold value may not be appropriate for different plant species and/or different locations (Tan et al., 2011). Fixed threshold methods can be sensitive to nonvegetation-related variations in the VI time series, which can result in considerable errors in the phenology timing estimates. Dynamic thresholds, which are established directly from the VI data characteristics over the study area are more customized because the threshold accounts for differences among vegetation types or the interannual variation of vegetation that occur within the targeted area.

However, these dynamic thresholds might not be stable over time and can be sensitive to the noise (White et al., 1997). The "baseline year" method developed by Shabanov et al. (2002) is based on the value from a selected baseline year in the time series to represent the normal phenological behavior of vegetated landscape and phenological events for other years are detected when time series values reach the values from the baseline year (Shabanov et al., 2002). However, the baseline year method is sensitive to the interannual variations and the selection of a representative year is subjective and challenging.

3.1.2. Change detection methods

Change detection methods determine the phenological dates by directly detecting the changing characteristics of the VI time-series curve such as the point with largest derivative or the inflection point with the local extreme in the first derivative or the rate of change of curvature (Fig. 3). It is assumed that the SOS and the EOS can be determined as the time starting the maximal increase or the time marking the maximal decrease in VI during the green up and senescence phases of the growing season, respectively. The primary difference among existing methods is how they determine the points with specific change characteristics in VI time series. Reed et al. (1994) proposed a moving averaged method to determine the SOS and the EOS as the dates that an observed VI time series crossed a curve established from moving average models, which is a milestone in the change detection method for estimating the SOS and EOS dates (Fig. 3a). Zhang et al. (2003) identified four key transition dates as the time point when the rate of change in curvature reaches a local minimum and maximum (Fig. 3b). Tateishi and Ebata (2004) determined the SOS and EOS as the time of the greatest increase and decrease in the VI time series, respectively (Fig. 3c).

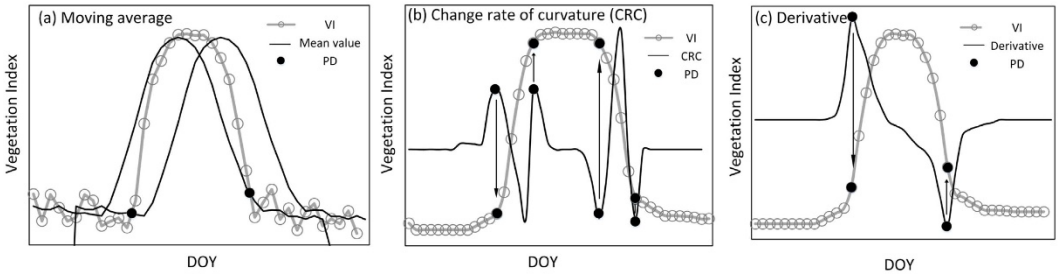

Figure 3. A schematic showing how phenological dates (PD) are extracted by detecting the changing characteristics of the VI time series curve using: (a) moving average method, (b) maximum and minimum values in the rate of change in curvature, and (c) the largest derivative.

Change detection methods are usually combined with curve fitting or data transformation methods to extract the phenological features from the smoothed data, as the fitted time series data are continuous in first derivative or change rate of curvature. Change detection methods were widely used in previous studies and considered an effective way to extract the phenological metrics for general vegetation types and coarse spatial resolution image pixels comprised of mixed vegetation types (Tateishi and Ebata, 2004; Zhang et al.,

2003; Moulin et al., 1997). The reliability depends on the assumption that the phenological stages (e.g., SOS and EOS) are corresponding to the rapid changes of VI values and the smoothed time series data approximates the true phenological characteristics of the vegetation. However, these methods may fail to determine the SOS and the EOS when it does not appear as an abrupt and rapid increase or decrease at greenup/senescence stage (de Beurs and Henebry, 2010), which is often encountered for vegetation types with less seasonal, spectral variation and more platykurtic-shape time series VI curves. It is unreliable to identify the phenological dates from inflection points filtered by these methods such as the BISE (Viovy et al., 1992) and TWO (Park et al., 1999) methods that filter time series data using linear interpolation methods and have discontinuities in first derivative or change rate of curvature. In addition, change detection methods focusing on the local change characteristics are also sensitive to the noise of remote sensing observation (Sakamoto et al., 2010).

3.2. Specific vegetation phenology detection methods

Motivated by the improvement of satellite instruments and demand of precise monitoring, there has been an increasing number of efforts to develop methods to estimate specific physiological-related phenology stages of vegetation types, particularly for crops (Pan et al., 2015; Sakamoto, 2018a,b; Sakamoto et al. 2005, 2010; Xu et al., 2017; Zeng et al., 2016; Zhao et al., 2011). Phenology studies for species-specific vegetation types provide valuable information for vegetation types classification and targeted plants monitoring and management as well as global food issues.

Some studies used above LSP detection methods to estimate the general phenological stages of species-specific vegetation (e.g. SOS, EOS) (Boschetti et al., 2009; Lu et al., 2014; Zheng et al., 2016; Antonucci et al., 2017; Onojeghuo et al., 2018). For example, Lu et al. (2014) identified the SOS of winter wheat as the time of maximum derivative of the time-series NDVI curve in the North China Plain. Zheng et al. (2016) detect the SOS and EOS for winter wheat and corn in China based on a ratio of in-season minimum NDVI to maximum NDVI. These methods regard the specific vegetation types as general vegetations and provide general seasonal information of the specific vegetation types, regardless of the physiological-based phenological stages. However, LSP methods cannot necessarily meet the requirement of precise monitoring and management of specific vegetation types, especially for crops. As a result, many phenology-monitoring methods focusing on the extraction of specific physiological-related phenology stages were proposed, which were discussed in this section.

The main methods for specific physiological-related phenology stage extraction can be classified into three categories (Table 4): (1) empirical methods, (2) phenology matching methods, and (3) simulation-based methods.. These three categories of methods are tailored for the estimation of physiological-based, phenological stages of specific vegetation types (e.g., corn (*Zea mays*)).

Table 4. Summary of main phenological metrics extraction methods for species-specific vegetation types from satellite imagery

Methods	Vegetation types	Sensors	Stage classification	Specific stages	Method classification	Reference
Line segment fitted parameters and statistics	*Quercus petraea*, *Fagus sylvatica* L.	AVHRR	Physiological-based phenological stages	Budburst, senescence	Empirical statistics method	Duchemin et al., 1999
Inflection points determined by derivative	Rice	MODIS	Physiological-based phenological stages	Planting, heading, and harvesting	Empirical method	Sakamoto et al., 2005
Based on the parameters derived from the best fitted polynomial curve	Potato	MODIS	General phenological stages	12 metrics for potato	Empirical method	Islam and Bala, 2008
Use TIMESAT software to detect rice phenological stages	Rice	MODIS	General phenological stages	Start, peak, and end of season	Empirical method	Boschetti et al., 2009
Derive phenological dates based on the optimum scaling parameters and shape model	Corn and soybeans	MODIS	Physiological-based phenological stages	8 stages for corn and soybeans, respectively	Phenology matching	Sakamoto et al., 2010
Regress the ground measure degree days and VI values	Sugarcane	ASTER	Physiological-based phenological stages	6 stages	Simulation	Mobasheri et al., 2010
Match the satellite-derived metrics with field observation and find the matching pairs	Corn and soybeans	MODIS	Physiological-based phenological stages	4 stages for corn, 4 stages for soybeans	Phenology matching	Zhao et al., 2011
Identified the start and peak of the season as the time of maximum derivation of time-series NDVI curve and maximum NDVI value, respectively	Winter wheat	SPOT	General phenological stages	The start and peak of the season	Empirical method	Lu et al., 2014
Threshold depending on the most probability	Wheat and corn	HJ-1 A/B	Physiological-based phenological stages	3 stages for wheat, 3 stages for corn	Empirical method	Pan et al., 2015
Integrate geophysical and remote sensing data into a regression-tree model	Cheatgrass	MODIS	General phenological stages	Start of season	Regression-tree method	Boyte et al., 2015
Combine the method of Sakamoto et al. (2010) and crop simulation model	Corn and soybeans	MODIS	Physiological-based phenological stages	8 stages for corn and soybeans, respectively	Phenology matching and simulation	Zeng et al., 2016
Calculate the optimum threshold of NDVI based on ratio of in-season maximum and minimum NDVI	Corn and winter wheat	SPOT5, MODIS	General phenological stages	Start and end of season	Empirical method	Zheng et al., 2016
Detect the inflexions of the fitted piecewise logistic curves	Oak, grass	MODIS, VIIRS, Landsat	General phenological stages	4 stages for grass and 4 stages for oak	Change detection	Liu et al., 2017
Optimized the settings of BISE, smoothing algorithms and thresholds on the calibration dataset	Wheat, barley, oilseed rape, and sugar beet	MODIS	Physiological-based phenological stages	3 for cereals and barley, 2 for oilseed rape, and 1 for sugar beet	Empirical method	Xu et al., 2017
Use multiclass relevant vector machine to conduct phenology estimation as a classification problem	Rice	HJ-1A/B, RADARSAT	Physiological-based phenological stages	6 stages	Machine learning	Yang et al., 2017

Table 4. *Continued*

Methods	Vegetation types	Sensors	Stage classification	Specific stages	Method classification	Reference
Use several methods (threshold, derivative and inflection point method) to detect three stages based on smoothed VI curves	Mangrove	MODIS	General phenological stages	Start, peak, and end of season	Empirical method	Guzman et al., 2018
Refined shape model fitting method entailed the calibration procedure without ground-based observations	8 crop species	MODIS	Physiological-based phenological stages	36 stages	Phenology matching	Sakamoto, 2018a,b

3.2.1. Empirical methods

Several researchers found that some physiological-based phenology metrics of specific vegetation types could be extracted by using physiological-based phenological information observed in the field to calibrate general LSP methods based on statistical data and empirical knowledge (Sakamoto et al., 2005; Liang et al., 2011; Han et al., 2018). For example, Pan et al. (2015) detected the key growth stages of wheat and corn through the application of thresholds to probability of occurrence values. Xu et al. (2017) estimated key phenological stages of sugar beet, wheat, oilseed rape, and barley by optimizing the settings of BISE, thresholds and smoothing algorithms based on the calibration dataset of ground-based, crop growth stage observations. Sakamoto et al. (2005) extracted the planting, heading, and harvesting stage of rice by detecting inflection points (the second derivative equals 0). Empirical methods for species-specific phenology studies are easy to apply; however, the process is subjective, and it can be difficult to correctly and rationally define these "user-defined" thresholds or feature points to get an unbiased estimation of phenological metrics.

3.2.2. Phenology matching methods

Phenology matching methods aim to match ground-based phenological stages with certain trajectory features within the satellite-derived VI time series curves. The rationale is that the phenological stages of specific vegetation types correspond to key points along the seasonal trajectory of time-series VI over the growing season can be identified through the "temporal matching" with ground-based phenology observations of these specific events (Sakamoto et al., 2010; Zhao et al., 2011; Zeng et al., 2016).

A prime example is the Two-Step Filter (TSF) approach (Sakamoto et al., 2010) that demonstrated several specific agronomic stages of corn and soybeans could be estimated by establishing the relationship between ground-based, agronomic stages of these crops and VI time-series data by deriving optimum parameters that approximate the fit of shape model to the smoothed VI data (eq. 5 and Fig. 4). The phenological dates are estimated from the preliminary determined phenological dates (based on visual observations) and the optimum scaling parameters (eq. 6). This method was designed to be an objective and unbiased approach for extracting specific phenological, crop growth stages by the direct relation to actual ground observations of these events. However, this approach is based on an assumption that the positions of crop phenology dates on the time-series VI curve are relatively fixed and the curve is linearly scalable through geometrical scaling, regardless

of key factors that influence the crop's annual growth progress (Sakamoto et al., 2010; Zeng et al., 2016).

$$g(x) = yscale \times h(xscale \times (x0 + tshift) + 0.5) - 0.5 \quad (5)$$

$$xest = xscale \times (xo + tshift) \quad (6)$$

where $h(x)$ is the shape model and $g(x)$ is fitted shape model. *xscale*, *yscale*, and *tshift* are scaling parameters. *Xest* and X_0 are the estimated phenological date and a preliminary defined phenological date respectively.

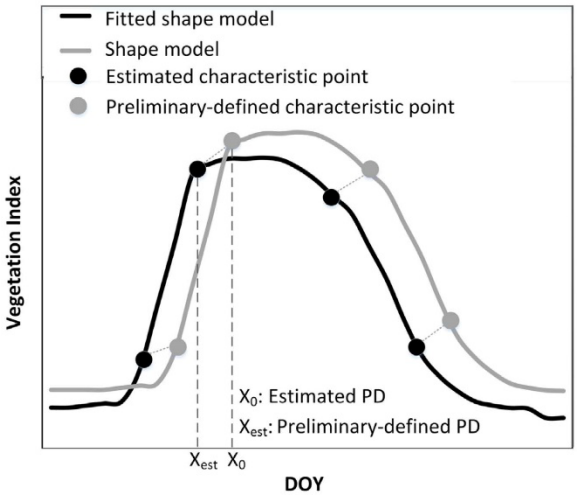

Figure 4. A schematic showing how phenological dates (PD) of species-specific vegetation are extracted by Two-Step Filter (TSF) approach (figure from Sakamoto et al., 2010). The estimated PD (X_{est}) is estimated from the optimum scaling parameters (xscale, tshift, yscale) and the preliminary determined phenological date (eqs. 5 and 6).

Phenology matching methods enable specific phenological events such as crop growth stages to be estimated and hold the advantage of minimizing the influence of localized fluctuations from errors and noise in the VI data (Sakamoto et al., 2010). However, if considerable variability of phenological stages occurs among different years and across different locations used to calibrate the matching method, the estimation accuracy of specific crop growth stages dates can be reduced (Zeng et al., 2016; Xu et al., 2017). As phenology matching method is typically based on the whole time series rather than more localized windows in the series, increased interannual variability of a specific phenological stage(s) can increase the uncertainty introduced by geometrical scaling of the whole time series when matching the phenological stages. The parameterization of the matching models also have to be adapted for different vegetation types and study areas (Xu et al., 2017), which requires ground-based phenological stages for calibration. Lastly, the accuracy and precision of the ground observations, as well as the sample size of observations (i.e., number of

years and locations), can directly influence the phenology detection accuracy when using these types of approaches.

3.2.3. Simulation-based methods

Simulation-based methods refer to those that use mechanism models to simulate phenological development. When the concept of heat units was introduced since 1730, many physical-based models, e.g. growing degree-days (GDD) measuring heat units (Mcmaster and Wilhelm, 1997; Mobasheri et al., 2010), crop models drived by meteorological factor (Brisson et al., 2003; Jones et al., 2003), ecosystems simulation models (Nemani et al., 2009), etc., have been widely used for plant phenology and development simulation and prediction. These models are helpful for analyzing the states of vegetation that may result from various forcings, such as climate conditions and soil environment (Nemani et al., 2009).

However, these simulation models are generally based on ground-measured observations in limited spatial coverage. Many approaches incorporating remote sensing data and the simulation concept of physical-based models have been used for phenology study over large geographic areas. For example, Nemani et al. (2009) monitor and forecast the vegetation phenology of the protected area (PA) ecosystems using a modeling framework that integrate satellite data, microclimate mapping and simulation models. Mobasheri et al. (2010) estimated phenological dates of sugarcane based on the regression between VI and GDD and stated that based on this method, any phenological stage of sugarcane can be identified with an acceptable precision (Mobasheri et al., 2010).

Particularly, widely used crop models can simulate phenological stages based on meteorological conditions (i.e., cumulative temperature or photoperiod) (Brisson et al., 2003; Jones et al., 2003). The combination of crop models and remotely sensed image data enable large-scale, regional monitoring and also can improve the accuracy of phenology date estimates compared to phenology matching methods using remote sensing data only (Zeng et al., 2016). Vintrou et al. (2014) demonstrated that the combined use of crop model and remotely sensed indicators provide a better estimate of crop phenology in the data-scarce West African countries (Vintrou et al., 2014). Zeng et al. (2016) incorporated crop models and phenology match method to detect the phenological stages of corn and soybeans. The study showed that the simulated vegetation growth rate based on a temperature and photoperiod response function was more relevant to growth dynamics of both crop types than the calendar (day of year, DOY) and minimized the influence of inter-annual climatic fluctuations that can negatively affect VI-based crop phenology methods (Zeng et al., 2016).

Simulation-based methods represent an option to improve the accuracy of satellite-derived phenological metrics. However, the application of physiological-process based simulation models can be challenging for several reasons. First, simulation models require reliable, station-based meteorological data, which can be difficult to obtain over large geographic areas where such in-situ observations are often lacking and comparable satellite-based observations often contain a degree of uncertainty that can reduce model performance (Zeng et al., 2016). Second, simulation models usually need to be calibrated for a specific cultivar/variety, which is likely to be unknown when working across large geographic areas compared to the traditional field scale that these models are typically applied. Lastly, simulation models generally perform well under ideal conditions but may

perform poorly when the vegetation is under stress (Malik et al., 2017; DeJonge et al., 2011). For example, water stress can significantly influence the growth progress of some species (Sokoto M. B. et al., 2015; Hodges, 1991), but it is still challenging to quantify the effect of water stress on plants' phenology development (McMaster et al., 2008; Zeng et al., 2016).

4. Discussion

As for general vegetation phenology detection, the SOS/EOS dates can be derived using different and widely varying methods. The first consideration is the specific phenology definitions and criterion of different methods to estimate SOS/EOS, which can be different even though the same name (SOS and EOS) is used to describe these metrics (de Beurs and Henebry, 2010; Sakamoto, 2018a,b). This ambiguity generates a wide discrepancy in the timings estimated for these metrics among these methods, making them difficult to compare and determine the most applicable method for a specific use (deBeurs and Henebry, 2010). For example, White et al. (2009) tested ten SOS estimation methods for North America and found the SOS estimates varied extensively within and among methods (by about 60 days). de Beurs and Henebry (2010) tested 12 common methods to extract SOS and EOS in the middle of North America and found the dates estimated by these different methods to vary by as much as 100 days. As a result, careful consideration should be taken in comparing and interpreting the results from different methods. The choice of the most appropriate model depends upon the purpose of the study, the growth trajectory to be analyzed, and the targeted land cover type(s). It is vital to establish a coherent nomenclature and establish a robust, quantitative method that best signifies the phenology of a wide variety of land cover types for global terrestrial LSP products to enable the analysis and comparison among different methods (de Beurs and Henebry, 2010).

In addition, a variety of factors can also have an impact on the phenology detection for both general and specific land cover types that include: (1) noise artifacts in remotely sensed time-series data, (2) intrinsic limitations of method selected, and (3) spatial scale differences between the phenological observation dates of individual plants/species and the mixed spectral signal observed from space in moderate to coarse spatial resolution imagery commonly used for this application. The impacts of these factors, the challenges in current studies, and the opportunities in the future are discussed in following sections.

4.1. Remote sensing data

The first consideration regarding satellite-derived remote-sensing data is temporal and spatial resolution. Temporal resolution is very important considering that phenological changes occur rapidly and cloud cover contamination issues of the optical satellite observations further reduce the number of images available to adequately detect phenological events (Gao et al., 2017; Walker et al., 2014; Yang et al., 2016). A limited number of observations during the growing season with good quality can result in large uncertainties in phenology date estimate or even cause failures in phenology detection (Yan et al., 2016a). As a result, temporally-composited AVHRR and MODIS data sets, with a consistent high temporal resolution time series of data, are widely used for phenology studies. Daily time series of images for defined time interval (e.g., 8 or 16 days) are commonly temporally

composited to generate a representative, cloud-free image for the temporal composite period. As for cloud-prone regions (e.g. tropical forest), the sensors on geostationary satellites (Yan et al., 2016a; Guan et al., 2014) with more frequent diurnal scanning than polar-orbiting sensors and microwave (Tong et al., 2019) minimally affected by cloud and aerosol contamination were reported to be promising for phenology study.

While, it also has been recognized that the main source of uncertainty and biases to derive phenology information from satellite imagery is the coarse spatial resolution (Zhang et al., 2009; Guan et al., 2014). Usually coarse phenology retrievals scaled poorly relative to the high-resolution equivalents, as the occurrence of multiple species within a grid cell can result in mixed spectra and need to be interpreted with care, particularly in heterogeneous areas (Vrieling et al., 2017; Zhang et al., 2017b).

So, the key point is how to balance the requirement of high temporal and spatial resolution. When the number of cloud-free observations is below the minimum quantity needed to characterize the basic trajectory of vegetation growth and key phenological transition stages, temporal resolution becomes the most important factor and the uncertainty in phenology detection increases substantially (Melaas et al. 2013, 2016). The minimum number of growing season observations needed to adequately capture the seasonal growth cycle of vegetation is not absolute and depends on the timing of cloud-free imagery and the type of vegetation being observed. The addition or elimination of imagery at different times during the growing season can have varying effects depending on the timing of the observation relative to the vegetation cycle of a given location. The effects may be significant when cloud-free imagery in not available at specific phenological stage (e.g., peak greenness) or during a key transition stage in the vegetation growth trajectory such as SOS or EOS (Vrieling et al., 2018).

When an adequate number of cloud-free images are available, spatial resolution is a key factor to consider in phenology detection given that medium to coarse spatial resolution imagery from sensors such as AVHRR and MODIS are composed of pixels containing a heterogeneous mosaic of multiple land cover types with varying phenological signals. Coarse resolution data limits the extraction of specific phenological stages for specific land cover types given this sub-pixel land cover heterogeneity (Fisher et al., 2006; Katharine et al., 2014). However, the spectral-temporal signal at the coarse spatial sale is more stable over longer periods of times because the land cover composition within pixels at a resolution of 1 km or lower remains relative static from year to year compared to higher spatial resolution pixels (e.g., 30 m) that detect common short-term land cover changes such as crop rotations. In general, satellite imagery with higher spatial resolution should be selected for species-specific vegetation phenology detection or in the areas with spatial heterogeneous landscapes, although some studies using MODIS to detect phenology of specific vegetation types in homogeneous areas have been published (Sakamoto et al., 2010; Zeng et al., 2016; Xu et al., 2017; Sakamoto, 2018a,b).

There is a trade-off between temporal and spatial resolution when using a single source of satellite imagery. However, three pathways have been suggested in the literature to help address this issue that include: (1) joint analysis of multi-year, high-resolution image acquisitions (Fisher et al., 2006; Melaas et al. 2013, 2016), (2) analysis of fused data from multi-resolution imagery acquired by different sensors (Gao et al., 2017; Yang et al., 2016; Walker

et al., 2014), and (3) combining image data with similar spatial resolution from multi-sensors by intercalibration can also improve phenological detection from a singleseason, high-resolution image time series (Vrieling et al., 2017). In particular, observations from comparable sensors (e.g. SPOT5 and RapidEye (Vrieling et al., 2017), Landsat and Sentinel (Pastick et al., 2018; Zhou et al., 2019), and from the single sensor over areas two scanning paths overlap (Wulder et al., 2019; Sun et al., 2017; Vrieling et al., 2018; An et al., 2018), can double the effective temporal resolution of imagery available and increase the temporal density of imagery in the time series for phenology detection directly using satellite imagery with a higher spatial resolution from sensors that have less frequent revisit times.

Multi-year, joint analysis is another option that is achieved by combining multi-year imagery observed from single sensor (e.g., Landsat) during different parts of the growing season to build a complete vegetation growth trajectory that can even be adjusted annually based on sparser individual-year observations (Fisher et al., 2006; Melaas et al. 2013, 2016). However, cloud cover around transition dates can still be problematic for annual adjustments, particularly for the land cover types that have minimal seasonal variability in greenness and/or strong year-to-year variations (Vrieling et al. 2017, 2018; Nijland et al., 2016).

Data fusion is being increasingly used to generate time series with high temporal and spatial resolutions (Gao et al., 2015; Walker et al., 2014; Zheng et al., 2016). Data fusion algorithms are expected to generate fine resolution synthetic images based on infrequent observations at fine resolution and relatively frequent coarse remote sensing data with relatively higher temporal resolution. However, the spectral and changes information at fine resolution are missing for most of the growing season, considering the general low temporal resolution of fine imagery. The data fusion algorithms are unavoidably based on some basic assumptions, such as the data from different sensors consistent and comparable and the changes in fine pixels equivalent to or proportional to changes in the corresponding coarse pixels, which can introduce uncertainty, especially in heterogeneous areas with high variability of change rates on the surface (Zhu et al., 2010; Gao et al. 2015, 2017; Emelyanova et al., 2013). In addition, the changes that are not recorded (e.g., due to clouds) or not sensible (too small) in the coarse resolution images cannot be reconstructed by data fusion algorithm, particularly when they occur at sub-pixel ranges (Gao et al., 2015). The spatial variation of phenological change from fused data need to be interpreted with care to validate it if it reflects "real" changes in vegetation phenology or if some variations in the time series data is related uncertainty introduced by the data fusion algorithm, especially in the heterogeneous area.

Besides cloud contamination, satellite-derived remote sensing data can also suffer from other types of uncertainties: (1) The VI data derived from sensors such as AVHRR, which have long historical records recorded by a series of sensors on different platforms over time, contains some data inconsistency because of sensor shifts between platform/sensors, as different platforms may have different solar altitude angle (SZA) (Nagol et al., 2014; Ji and Brown, 2017). Derived VI is sensitive to the changes in SZA, thereby introducing substantial uncertainties in phenological metrics and trend analysis results (Ji and Brown, 2017; Tian et al., 2015; Nagol et al., 2014; van Leeuwen et al., 2006). (2) Sensor degradation can also introduce uncertainties and inconsistencies into time-series data sets for sensors that are used over a long period of time. For example, nonnegligible sensor degradation

ratio between NOAA AVHRR Channels 1 and 2 has been quantified in previous studies (Los, 1998; Wu, 1993). In addition, the Terra MODIS sensor has demonstrated sensor degradation, especially for the visible blue band used for atmospheric correction of the other MODIS multispectral bands, leading to a decreasing trend in retrieved aerosol optical depth and resulting in a decline in NDVI values in MODIS collection 5 (C5) data products (Wang et al., 2012). This small, negatively biased sensor degradation in C5 NDVI data may be confused as a real browning trend over vegetation, which is more difficult to interpret than cloud contamination or other sensor artifacts that usually result in a sudden drop in the VI data time series (Wang et al., 2012; Zhang et al., 2017c). (3) An integration of comparable sensors requires a proper intercalibration that is effective across seasons and land cover classes and can introduce uncertainty, too (Zhou et al., 2019; Vrieling et al., 2017; Wang et al., 2015).

4.2. Data smoothing and phenology detection methods

Data smoothing methods are expect to maintain the integrity of vegetation dynamics while removing the noise component (Hermance, 2007; Cao et al. 2015, 2018; Beck et al., 2006; Hird and Mcdermid, 2009). Fitting the time series from satellite imagery within local windows or using high-order harmonic series or more parameters can capture the vegetation dynamics better, especially for irregular, asymmetrical, shaped VI curves (e.g., a plateau in growth peak period). However, these methods tend to be more sensitive to local fluctuation and data noise. In comparison, methods based on the entire annual time series or low-order harmonic series often obtain a smoother curve but may deviate from actual vegetation growth trajectory and have overcorrection problems (dampen the actual vegetation fluctuations). Currently, it is difficult to determine the "best" method for all situations and the selection of the most appropriate method should consider the targeted phenological metrics, the biogeographical characteristics of the study region, potential noise sources in the VI data (e.g., strength and nature) and the general shape of time series VI curves (Hird and Mcdermid, 2009; Cao et al., 2015).

Satellite sensors do not directly record specific phenological events but rather a general measure of vegetation activity and growth at the pixel scale (Atkinson et al., 2012), and the derived phenology should be considered to be related, but not identical, to traditional visual observations of plant phenology (Verhegghen et al., 2014), which is a common limitation for remote sensed-based phenology monitoring methods (White and Nemani, 2006; Atkinson et al., 2012; Verhegghen et al., 2014; de Beurs and Henebry, 2005). As a result, VI changes derived from satellite observations may not always directly reflect the physiological process of vegetation. Understanding and distinguishing the changes in response to biotic from abiotic environmental perturbations is still a challenge in remote sensing phenology studies (Beurs and Henebry, 2010). For example, some methods use the time of the largest increase in the NDVI to indicate SOS, but this is problematic in persistently snow-covered areas such as the higher latitudes, where snow melts yield a similar NDVI response to SOS in other parts of the world (Delbart et al. (2005a,b); Reed et al., 1994). For grasslands, annual and interannual NDVI changes may reflect grazing practices in addition to regional climatological patterns (Hall-Beyer, 2003). The EOS metric can be misidentified during an extended period of cloudiness, instead of corresponding to actual senescence

(de Beurs and Henebry, 2010). An early bias in the greenup onset date detection for corn and soybeans was found to be introduced by pre-crop NDVI signals from the extensive weed or volunteer crop cover that commonly precede the planting of crops (Wardlow et al., 2006). The vegetation change caused by disease, water stress or N stress may be confused with real onset of leaf senescence (Viña et al., 2004). Small seasonal VI variations of evergreen vegetation (e.g., needleleaf forests) make it challenge for phenological event extraction (Melaas et al., 2013; Guyon et al., 2011) compared to deciduous forest canopy which have more clearly defined seasonal responses in the VI data record (Melaas et al., 2013; Liu et al., 2016; Garrity et al., 2011).

Hou et al. (2014) proposed a method that detects phenology from the cumulative NDVI, which is not sensitive to short-term disturbances (e.g., insect attack or severe drought). It is an effective way to reduce the influence of short-term fluctuations or noise, but dampens subtle VI changes of the targeted vegetation as a tradeoff. Several studies suggested to combine multiple indices, multiple sensors and/or multiple data sources to quantitatively describe annual patterns of vegetation phenology as an alternative (Wu et al., 2014; Gonsamo et al., 2012; Garrity et al., 2011).

Several studies have used existing software tools to analyze VI time series data for phenology-related studies (Jia et al., 2014; Rodrigues et al., 2013; Heumann et al., 2007) that include TIMESAT (Jönsson and Eklundh, 2004), Phenological Parameters Estimation Tool (PPET (Mckellip et al., 2010);), enhanced TIMESAT (Tan et al., 2011), Time-Stats (Udelhoven, 2011), Phenosat (Rodrigues et al., 2012), Hants (Zhou et al., 2015), CropPhenology (Araya et al., 2018), and QPheno-Metrics (Duarte et al., 2018). These software tools provide free functionalities for the reconstruction of time series data and extraction of phenological information customized with a number of user-defined input parameters based on the VI time series data. They are applicable in data reconstruction providing multiple common data-smoothing methods like logistic models, Savitzky-Golay, asymmetric Gaussian functions, piecewise regression, Fourier transforms, and so forth, and generally perform well in general LSP extraction (e.g., SOS, EOS) providing common extraction methods, such as threshold method and inflection method (White et al., 2009; Rodrigues et al., 2013; Boschetti et al., 2009; Eklundh and Jönsson, 2015).

However, they are generally limited in physiological growth stages extraction of species-specific vegetation due to the unclear relationship between the derived metrics and physiological growth stages (Araya et al., 2018). For example, TIMESAT, the most widely used software for data smoothing and phenology detection, provides only threshold method for seasonal metrics extraction (11 metrics, focusing on general LSP, e.g., SOS, EOS) based on fitted functions (Boschetti et al., 2009; Eklundh and Jönsson, 2012). Araya et al. (2018) recently presented the CropPhenology package to extract crop phenology metrics from VI time series and included new metrics related to the crop yield (e.g., the curve integral before and after maximum VI). However, it is still limited in phenology detection of species-specific vegetation related to the physiological growth stages. In addition, these tools, relying on the time series VI data recording the complete vegetation growth cycle, are general not applicable for real-time or short-term phenology prediction.

4.3. Scale effect

Scale effect refers to the phenomenon that the value of a phenological metric extracted from coarse spatial resolution satellite imagery does not necessarily equate to the average of the metric at a higher resolution within the same geographic footprint (Zhang et al., 2017b; Peng et al., 2017). As a result, satellite-based phenology detection result can be influenced by the spatial scale of the remote sensing observation. In addition, vegetation phenological metrics extraction from satellite imagery highlights the calibration and validation using ground observations at site level, including field visual observations and near-surface measurement. However, the incompatibility of spatial scales between satellite-based observations aggregating signal of canopy within the grid cell and field observation of individual plants introduces uncertainty (Liang et al., 2011; Zhang et al., 2017b; Moura et al., 2017; Fisher and Mustard, 2007).

Several studies have investigated the scale effect (Peng et al. 2017, 2018; Berra et al., 2019; Zhang et al., 2017b; Chen et al., 2018). Several spatial upscaling techniques to produce a phenological representation at the landscape level that are spatially comparable to the scale of satellite signals have been proposed to help address the spatial scale gap between ground- and satellite-based observations (Liu et al., 2015; Verhegghen et al., 2014; Liang et al., 2011; Zhang et al., 2017b). For example, Zhang et al., 2017b suggested "percentile aggregation" method that the timing of the 30th percentile is considered to be biophysically meaningful for SOS detection, rather than simple aggregation approaches such as majority filtering, or averaging (Ganguly et al., 2010; Delbart et al., 2015; Zhang et al., 2017b), as SOS becomes detectable based on remote sensing data after a certain amount of leaves within the coarse resolution pixel start to emerge (Zhang et al., 2017b). However, work still remains to integrate the species-based, leaf-level phenology to canopy-level phenology to calibrate and validate remote-sensing-based vegetation phenology, which is also in accordance with the goal of ground-based observation programs such as the National Ecological Observatory Network (NEON) (Thorpe et al., 2016). Other remaining key issues to be investigated include: the systematic difference in the phenology metrics detection results derived from multiple scales, identifying the factors accounting for the scale effect (Liu et al., 2019) and understanding the mechanism(s) underlying the scale effect and the quantitative description of the scale effect.

Near-surface imagery acquired by PhenoCams or sensors on other close-range platforms such as unmanned aerial vehicles (UAVs) using optical principles similar to those used by sensors carried on satellites can help bridging the spatial mismatch between field and satellite data and improve our standing of underlaying phenological process and mechanism (D'Odorico et al., 2015; Moura et al., 2017). However, when comparing the phenological results from satellite-based and near-surface retrievals, attention should be paid not only to the mixed spectra within a grid cell but also the different vegetation indices and different viewing angles of the observations (Berra et al., 2019; Hufkens et al., 2012). Near-surface sensors, except for the sensor carried on unmanned aerial vehicle (UAV), are often oriented with a view angle closed to be horizontal. As a result, these near-surface sensors receive a higher contribution from the understory vegetation and smaller contribution from the canopy top (Peltoniemi et al., 2018; Berra et al., 2019; Hufkens et al., 2012; Liu et al., 2017a). While UAVs acquire ultra-high spatial resolution data at a near-nadir-

view angle at user-defined revisit interval and detecting vegetation phenology in a manner similar to satellite sensors is promising for fine-scale measurement of vegetation phenology as well as satellite-based phenological products validation (Berra et al., 2019; Zhang et al., 2018b; Klosterman et al., 2018).

In addition, combined methods that incorporate remote sensing data and physical/empirical models offer great potential for improving vegetation phenology detection at larger, regional scales. Physical models have explicit mechanisms that can simulate the phenological stages on the basis of individual plant (White et al., 2009; Zeng et al., 2016). The incorporation of remote-sensing data and physical models fill the scale gap between the pixel and plants and help us understand vegetation growth progress. In addition, simulation models based on the empirical relationship between vegetation phenological events (e.g., Spring indices model (Lieth and Schwartz, 1997)) and the driving factors such as temperature, moisture, photoperiod, or carbon exchange (e.g., Canadian Terrestrial Ecosystem Model (Arora and Boer, 2005)) offer alternative reference data sets that can be used in remote-sensing phenology studies. However, these models are usually developed for a specific plant species or geographic region, and their extension to other areas or land-cover types requires a reparameterization of the methods, limiting their overall utility for widespread application in remote sensing phenology work.

4.4. Challenges and opportunities

Satellites remain the only feasible tool for continuous monitoring of Earth dynamics at regional to global scales (Berra et al., 2019; Liu et al., 2017a). There remain several challenges for both LSP and species-specific phenology detection using satellite imagery.

First, data contamination in the form of undetected subpixel clouds, residual thin clouds, cloud shadows on the landscape, and bidirectional effects can introduce uncertainty. It remains challenging to disentangle noise and feature points on the growth curve. A variety of data-smoothing methods to remove the data noise have been developed. It is still difficult to find the best data smoothing for all the vegetation types and areas (de Beurs and Henebry, 2010).

Second, phenological metrics detection accuracy varies among the different methods and needs to be further improved. First, most current methods are based on the feature point detection in terms of mathematical theories rather than a physiological basis, which limits the accuracy of specific phenolgical metrics detection. Second, different definitions and criterion among detection methods is a primary reason for the significant differences and incomparability of results among methods. Third, different spatial scales between the space and ground observations still impedes the connection between the broader vegetation community-level phenology patterns at the pixel level of satellite imagery and the data at the individual plant level from the ground. The scale effect remains challenging to understand how the species-specific phenological metrics are reflected in remote sensing phenology products. Future works emphasis the joint analyses of observation from multiple sources and multiple scales to bridge the relationship between remotely sensed phenology products and plant physiological processes, and improve our understanding of how the phenological transitions can be reflected from the pixel-level, spectral signal observed by sensors carried on satellite (Wingate et al., 2015; Migliavacca et al., 2011; Richardson et al.,

2007). Fourth, compared to the start of season, satellite-derived phenology development during vegetation senescence approaching the EOS remains poorly understood. The gradual change during the senescence phase for many vegetation types makes it more difficult to detect the transition dates of senescence. In addition, the fall phenological responses including foliage coloration and defoliation are more complicated compared to the vegetative, green-up stage during the SOS. Future studies are needed to explore the underlying processes and mechanisms of vegetation senescence. Combining multisources data is helpful for understanding the underlying process and detecting the specific phenological transition dates. For example, structural information collected from LiDAR sensors is helpful for distinguishing the foliage coloration and defoliation during the senescence phase.

Third, the number of ground-based observations are insufficient, especially in underdeveloped and developing countries that lack traditional phenological observing networks. Most existing networks, aside from those in Europe, selected locations in North America, and a few other countries, have a relatively short historical record and often have a limited number of stable, consistent monitoring locations. A need exists to build a systematic, long-term monitoring network globally with unifying standards of phenology measures and definitions, methods. Since automated digital cameras, providing consistent and continuous monitoring of vegetation canopy conditions at low cost allows phenology analysis similar to those applied with satellite imagery, visual interpretation of phenology dates from the photography and characterization for vegetation phenology at high temporal and spatial resolution. Digital cameras have been shown to be valuable tools to interpret, evaluate, and validate the phenology results derived from satellite imagery at the local and regional scales (Zhang et al., 2018; Sonnentag et al., 2012). Specifically, the PhenoCam network provides free, publicly accessible digital imagery at the continental level (Richardson et al., 2018). In the future, automated digital cameras are promising to address this gap regarding the insufficiency of ground observation globally.

Finally, real-time monitoring and short-term phenology prediction remain challenging. Short-term forecasting refers to the prediction before the occurrence of a phenological event, and real-time monitoring refers to the detection as detecting a phenological occurrence as it occurs (White and Nemani, 2006; Zhang et al., 2012; de Beurs and Henebry, 2010). Currently, most of the phenology studies focus on detection of historical phenology stages using time series recording the complete vegetation growth cycles. Little attention has been paid to short-term forecasting and real-time monitoring of vegetation phenology, which is very important for ecosystem forecasting, forest and crop management, food security, and numerical weather modeling (White and Nemani, 2006; Zhang et al., 2012; Zhang et al., 2018a). In previous studies, phenology prediction was typically based on a predefined threshold (White and Nemani, 2006), simulation models (Nemani et al., 2009; Zhang et al., 2012; Liu et al., 2017b), or regression models (Boyte and Wylie, 2018; Boyte et al., 2015). Challenges still remain to solve nearly intractable problems of highly noisy time series derived from satellite sensors based on the incomplete recording of the vegetation life cycle (White and Nemani, 2006; Zhang et al., 2012) and to develop reliable real-time and prediction phenology detection models independent of the full vegetation growth cycle.

Motivated by these challenges, there are also many potential opportunities for phenology detection from space. With recent breakthrough of space remote-sensing technology,

both temporal and spatial resolution of satellite imagery has being improved. Using the data from the new sensor to improve the accuracy of phenology detection will be a future trend. Recently launched sensor series like Europe's Sentinel and China's Gaofen series as well as emerging constellations such as CubeSats like Planet provide unparalleled opportunities for regional- to local-scale phenology monitoring. Specifically, Sentinel-2A and Sentinel-2B provide 10 m resolution multispectral image data at a 5-day interval. Collectively, imagery from Sentinel-2A, Sentinel-2B, and Landsat-8 can have higher temporal resolution (~3 days) (Claverie et al., 2018; Li and Roy, 2017). PlanetScope (PS) can provide daily global observations at higher spatial resolution (3 m) with about 170 CubeSats (small satellites), which is promising for reliably detecting phenological metrics in heterogeneous areas—for example, smallholder agricultural systems. In addition, the new generation of geostationary satellites at a spatial resolution of 0.5–1.0 km, such as Geostationary Operational Environmental Satellite-R Series (GOES-R) and Himawari-8, are promising for phenology studies, especially in low-latitude areas and other cloud-prone regions where data with very high temporal resolution (more frequent than daily) is preferred (Yan et al., 2016a; Guan et al., 2014).

The emerging near-surface measurements (e.g., fixed digital cameras, flux measurements, sensors carried by unmanned aerial vehicles, and smartphone cameras) offer promising options of providing high-resolution phenology observational data. An array of near-surface data sets collected by various observatory network platforms, such as ecosystem observatory network (e.g., National Ecosystem Observatory Network, NEON (Thorpe et al., 2016)), phenology observation network (e.g., PhenoCam Network (Richardson et al., 2011)), carbon flux observation network (e.g., FLUXNET (Friend et al., 2010)), are expected to offer long time-series ground-based observations for future phenology studies. It is also a future trend that the existing networks engage with the data/platforms from sensor webs, multiple institutes, and the public (e.g., smartphone) via network by data integration and standardization.

5. Summary

Satellite remote sensing observations have considerable potential for characterizing spatio-temporal patterns of vegetation phenology from local to global scale, thus enabling effective and unbiased monitoring of vegetation phenology in a consistent time- and cost-efficient manner. Vegetation phenology monitoring includes general vegetation phenology measures and species-specific vegetation phenology (e.g., flowering and silking stages). LSP represents "generic or mixed" vegetation phenological events, while species-specific vegetation phenology is usually associated with more traditional, physiological-based phenological events of specific vegetation types. LSP detection does not aim to detect phenological dates of specific species, nevertheless, disentangled phenology information of various specific species is preferred for LSP detection. As phenology information aggregated from multispecies introduce uncertainty for LSP. The majority of LSP studies focus on phenological patterns and their relationship with climatic variability (Adole et al., 2016), while most of species-specific vegetation phenology studies focus on crop growth stages

of, which is commonly used in monitoring of crop conditions, yield estimation, and precision farming management.

Quantifying phenological stages from remote sensing at regional scale is still a challenging task (Liu et al., 2016; Antonucci et al., 2017). It is particularly difficult to develop a data smoothing or phenology detection model that is universally applicable (Liu et al., 2016). Many factors like noise in remote-sensing data (e.g., viewing geometry, cloud or snow contamination, atmospheric conditions, and directional effects), uncertainty of ground observations, methods of data preprocessing and quality control, perturbations of biotic and abiotic environmental factors, and conversion of scale between individual plants and ecosystem-level phenology create various levels of uncertainties and introduce bias into the identification of vegetation phenological metrics (Jönsson and Eklundh, 2002; Kandasamy et al., 2013). Future work includes the establishment of robust data-fitting methods and phenological metrics detection methods. Specifically, machine learning methods show great potential in cloud data recovery, time series data reconstruction, and phenology monitoring.

Accordingly, definite relationship should be established between the ground-observed, physiology-based phenology at individual plants level and the satellite-derived canopy phenology at the pixel level with the aid of multiple-source and multiple-scale observations. Currently, scale effect among the phenology products derived at different scales is still challenging, which will be the research emphasis in the future studies. The improvement of both spatial and temporal resolution of recent launched or planed satellites such as sentinel series, small satellite constellation, and so forth, is promising for providing global finer phenology monitoring. In addition, the development and population of near-surface measurement offers great opportunities to provide ground truth phenological results at site level and helps us to understand satellite-based phenology detection mechanism and extent phenology detection to regional scale in the future.

Acknowledgments – We would like to thank Professor Jin Chen from Beijing Normal University for his enthusiastic support and helpful comments. We also thank three anonymous reviewers for their helpful comments. This work was supported by the National Nature Science Foundation of China program (Grant No. 41901353), the National Key Research and Development Program of China (Grant No. 2017YFC1502406-03), and the Fundamental Research Funds for the Central Universities (Program No. 2662019QD054).

References

Adole, T., Dash, J., Atkinson, P.M., 2016. A systematic review of vegetation phenology in Africa. Ecol. Inf. 34, 117–128.

Ahl, D.E., Gower, S.T., Burrows, S.N., Shabanov, N.V., Myneni, R.B., Knyazikhin, Y., 2006. Monitoring spring canopy phenology of a deciduous broadleaf forest using MODIS. Remote Sens. Environ. 104, 88–95.

An, S., Zhang, X., Chen, X., Yan, D., Henebry, G.M., 2018. An exploration of terrain effects on land surface phenology across the Qinghai–Tibet plateau using Landsat ETM+ and OLI data. Remote Sens. 10.

Antonucci, S., Rossi, S., Deslauriers, A., Morin, H., Lombardi, F., Marchetti, M., Tognetti, R., 2017. Large-scale estimation of xylem phenology in black spruce through remote sensing. Agric. For. Meteorol. 233, 92–100.

Araya, S., Ostendorf, B., Lyle, G., Lewis, M., 2018. CropPhenology: an R package for extracting crop phenology from time series remotely sensed vegetation index imagery. Ecol. Inf. 46, 45–56.

Arora, V.K., Boer, G.J., 2005. A parameterization of leaf phenology for the terrestrial ecosystem component of climate models. Glob. Chang. Biol. 11, 39–59.

Atkinson, P.M., Jeganathan, C., Dash, J., Atzberger, C., 2012. Inter-comparison of four models for smoothing satellite sensor time-series data to estimate vegetation phenology. Remote Sens. Environ. 123, 400–417.

Badhwar, G.D., 1984. Use of Landsat-derived profile features for spring small-grains classification. Int. J. Remote Sens. 5, 783–797.

Balzter, H., Gerard, F., George, C., Weedon, G., Grey, W., Combal, B., Bartholomé, E., Bartalev, S., Los, S., 2007. Coupling of vegetation growing season anomalies and fire activity with hemispheric and regional-scale climate patterns in central and East Siberia. J. Clim. 20, 3713–3729.

Beck, P.S.A., Atzberger, C., Høgda, K.A., Johansen, B., Skidmore, A.K., 2006. Improved monitoring of vegetation dynamics at very high latitudes: a new method using MODIS NDVI. Remote Sens. Environ. 99, 321–334.

Beck, P.S.A., Jönsson, P., Høgda, K.A., Karlsen, S.R., Eklundh, L., Skidmore, A.K., 2007. A ground-validated NDVI dataset for monitoring vegetation dynamics and mapping phenology in Fennoscandia and the Kola peninsula. Int. J. Remote Sens. 28, 4311–4330.

Berra, E.F., Gaulton, R., Barr, S., 2019. Assessing spring phenology of a temperate woodland: a multiscale comparison of ground, unmanned aerial vehicle and Landsat satellite observations. Remote Sens. Environ. 223, 229–242.

Beurs, K.M.D., Henebry, G.M., 2010. Spatio-Temporal Statistical Methods for Modelling Land Surface Phenology: Springer Netherlands.

Boschetti, M., Stroppiana, D., Brivio, P.A., Bocchi, S., 2009. Multi-year monitoring of rice crop phenology through time series analysis of MODIS images. Int. J. Remote Sens. 30, 4643–4662.

Boyd, D.S., Almond, S., Dash, J., Curran, P.J., Hill, R.A., 2011. Phenology of vegetation in Southern England from Envisat MERIS terrestrial chlorophyll index (MTCI) data. Int. J. Remote Sens. 32, 8421–8447.

Boyte, S.P., Wylie, B.K., 2018. Near-real-time herbaceous annual cover in the sagebrush ecosystem, USA. U.S. Geological Survey data release. https://doi.org/10.5066/ P9RIV03D

Boyte, S.P., Wylie, B.K., Major, D.J., Brown, J.F., 2015. The integration of geophysical and enhanced Moderate Resolution Imaging Spectroradiometer Normalized Difference Vegetation Index data into a rule-based, piecewise regression-tree model to estimate cheatgrass beginning of spring growth. Int. J. Digit. Earth 8, 118–132.

Brisson, N., Gary, C., Justes, E., Roche, R., Mary, B., Ripoche, D., et al., 2003. An overview of the crop model stics. Eur. J. Agron. 18 (3-4), 309–332.

Brown, M.E., de Beurs, K.M., Marshall, M., 2012. Global phenological response to climate change in crop areas using satellite remote sensing of vegetation, humidity and temperature over 26 years. Remote Sensing of Environment 11 (126), 174–183.

Brown, J., Wardlow, B., Tadesse, T., Hayes, M., Reed, B., 2008. The vegetation drought response index (VegDRI): a new integrated approach for monitoring drought stress in vegetation. GIScience Remote Sens. 45, 16–46.

Cai, Z., Jönsson, P., Jin, H., Eklundh, L., 2017. Performance of smoothing methods for reconstructing NDVI time-series and estimating vegetation phenology from MODIS data. Remote Sens. 9, 1271.

Cao, R., Chen, J., Shen, M., Tang, Y., 2015. An improved logistic method for detecting spring vegetation phenology in grasslands from MODIS EVI time-series data. Agric. For. Meteorol. 200, 9–20.

Cao, R., Chen, Y., Shen, M., Chen, J., Yang, W., 2018. A simple method to improve the quality of NDVI time-series data by integrating spatiotemporal information with the Savitzky-Golay filter. Remote Sens. Environ. 217, 244–257.

Chen, J., Jönsson, P., Tamura, M., Gu, Z., Matsushita, B., Eklundh, L., 2004. A simple method for reconstructing a high-quality NDVI time-series data set based on the Savitzky-Golay filter. Remote Sens. Environ. 91, 332–344.

Chen, J.M., Deng, F., Chen, M., 2006. Locally adjusted cubic-spline capping for reconstructing seasonal trajectories of a satellite-derived surface parameter. IEEE Trans. Geosci. Remote Sens. 44, 2230–2238.

Chen, X., Wang, D., Chen, J., Wang, C., Shen, M., 2018. The mixed pixel effect in land surface phenology: a simulation study. Remote Sens. Environ. 211, 338–344.

Claverie, M., Ju, J., Masek, G., Dungan, J.,L., J., F. Vermote, E., Roger, J., Skakun, S., Justice, C., 2018. The Harmonized Landsat and Sentinel-2 surface reflectance data set. Remote Sens. Environ. 219, 145–161.

Cleveland, W.S., Devlin, S.J., 1988. Locally weighted regression: an approach to regression analysis by local fitting. J. Am. Stat. Assoc. 83, 596–610.

D'Odorico, P., Gonsamo, A., Gough, C.M., Bohrer, G., Morison, J., Wilkinson, M., Hanson, P.J., Gianelle, D., Fuentes, J.D., Buchmann, N., 2015. The match and mismatch between photosynthesis and land surface phenology of deciduous forests. Agric. For. Meteorol. 214-215, 25–38.

Dash, J., Curran, P.J., 2004. Evaluation of the MERIS Terrestrial Chlorophyll Index. pp. 100–104.

Dash, J., Jeganathan, C., Atkinson, P.M., 2010. The use of MERIS Terrestrial Chlorophyll Index to study spatio-temporal variation in vegetation phenology over India. Remote Sens. Environ. 114, 1388–1402.

de Beurs, K.M., Henebry, G.M., 2004. Land surface phenology, climatic variation, and institutional change: analyzing agricultural land cover change in Kazakhstan. Remote Sens. Environ. 89, 497–509.

de Beurs, K.M., Henebry, G.M., 2005. Land surface phenology and temperature variation in the International Geosphere-Biosphere Program high-latitude transects. Glob. Chang. Biol. 11, 779–790.

de Beurs, K.M., Henebry, G.M., 2010. Spatio-Temporal Statistical Methods for Modelling Land Surface Phenology: Springer Netherlands.

DeJonge, K., Andales, A., Ascough II, J., Hansen, N., 2011. Modeling of full and limited irrigation scenarios for corn in a semiarid environment. Trans. ASABE 54, 481–492.

Delbart, N., Kergoat, L., Le Toan, T., Lhermitte, J., Picard, G., 2005a. Determination of phenological dates in boreal regions using normalized difference water index. Remote Sens. Environ. 97, 26–38.

Delbart, N., Kergoat, L., Toan, T.L., Lhermitte, J., Picard, G., 2005b. Determination of phenological dates in boreal regions using normalized difference water index. Remote Sens. Environ. 97, 26–38.

Delbart, N., Beaubien, E., Kergoat, L., Toan, T.L., 2015. Comparing land surface phenology with leafing and flowering observations from the PlantWatch citizen network. Remote Sens. Environ. 160, 273–280.

Diao, C., 2019. Complex network-based time series remote sensing model in monitoring the fall foliage transition date for peak coloration. Remote Sens. Environ. 229, 179–192.

Duarte, L., Teodoro, A.C., Monteiro, A.T., Cunha, M., Gonçalves, H., 2018. QPhenoMetrics: an open source software application to assess vegetation phenology metrics. Comput. Electron. Agric. 148, 82–94.

Duchemin, B., Goubier, J., Courrier, G., 1999. Monitoring phenological key stages and cycle duration of temperate deciduous forest ecosystems with NOAA/AVHRR data. Remote Sens. Environ. 67, 68–82.

Eilers, P.H.C., 2003. A perfect smoother. Anal. Chem. 75, 3631.

Eklundh, L., Jönsson, P., 2015. TIMESAT: A Software Package for Time-Series Processing and Assessment of Vegetation Dynamics. Springer International Publishing.

Eklundh, L., Jönsson, P., 2012. TIMESAT 3.2 with Parallel Processing-Software Manual. Lund University.

Elmore, A.J., Guinn, S.M., Minsley, B.J., Richardson, A.D., 2012. Landscape controls on the timing of spring, autumn, and growing season length in mid-Atlantic forests. Glob. Chang. Biol. 18, 656–674.

Emelyanova, I.V., McVicar, T.R., Van Niel, T.G., Li, L.T., van Dijk, A.I.J.M., 2013. Assessing the accuracy of blending Landsat-MODIS surface reflectances in two landscapes with contrasting spatial and temporal dynamics: a framework for algorithm selection. Remote Sens. Environ. 133, 193–209.

Fischer, A., 1994. A model for the seasonal variations of vegetation indices in coarse resolution data and its inversion to extract crop parameters. Remote Sens. Environ. 48, 220–230.

Fisher, J.I., Mustard, J.F., 2007. Cross-scalar satellite phenology from ground, Landsat, and MODIS data. Remote Sens. Environ. 109, 261–273.

Fisher, J.I., Mustard, J.F., Vadeboncoeur, M.A., 2006. Green leaf phenology at Landsat resolution: scaling from the field to the satellite. Remote Sens. Environ. 100, 265–279.

Friend, A., Arneth, A., Kiang, N., Lomas, M., Ogee, J., Rodenbeckk, C., Running, S., Santaren, J., Sitch, S., Viovy, N., 2010. FLUXNET and modelling the global carbon cycle. Glob. Chang. Biol. 13, 610–633.

Funk, C., Budde, M.E., 2009. Phenologically-tuned MODIS NDVI-based production anomaly estimates for Zimbabwe. Remote Sens. Environ. 113, 115–125.

Galford, G.L., Mustard, J.F., Melillo, J., Gendrin, A., Cerri, C.C., Cerri, C.E.P., 2008. Wavelet analysis of MODIS time series to detect expansion and intensification of rowcrop agriculture in Brazil. Remote Sens. Environ. 112, 576–587.

Ganguly, S., Friedl, M.A., Tan, B., Zhang, X.Y., Verma, M., 2010. Land surface phenology from MODIS: characterization of the Collection 5 global land cover dynamics product. Remote Sens. Environ. 114, 1805–1816.

Gao, B., 1996. NDWI—a normalized difference water index for remote sensing of vegetation liquid water from space. Remote Sens. Environ. 58, 257–266.

Gao, F., Hilker, T., Zhu, X., Anderson, M., Masek, J., Wang, P., Yang, Y., 2015. Fusing Landsat and MODIS data for vegetation monitoring. IEEE Geosci. Remote Sens. Mag. 3, 47–60.

Gao, F., Anderson, M.C., Zhang, X., Yang, Z., Alfieri, J.G., Kustas, W.P., Mueller, R., Johnson, D.M., Prueger, J.H., 2017. Toward mapping crop progress at field scales through fusion of Landsat and MODIS imagery. Remote Sens. Environ. 188, 9–25.

Garrity, S.R., Bohrer, G., Maurer, K.D., Mueller, K.L., Vogel, C.S., Curtis, P.S., 2011. A comparison of multiple phenology data sources for estimating seasonal transitions in deciduous forest carbon exchange. Agric. For. Meteorol. 151, 1741–1752.

Gitelson, A.A., 2004. Wide Dynamic Range Vegetation Index for remote quantification of biophysical characteristics of vegetation. J. Plant Physiol. 161, 165–173.

Gobron, N., Pinty, B., Aussedat, O.E.L., Chen, J.M., Cohen, W.B., Fensholt, R., Gond, V., Huemmrich, K.F., Lavergne, T., 2006. Evaluation of fraction of absorbed photosynthetically active radiation products for different canopy radiation transfer regimes: methodology and results using Joint Research Center products derived from SeaWiFS against ground-based estimations. J. Geophys. Res. Atmos. 111, 2943–2979.

Gonsamo, A., 2016. Circumpolar vegetation dynamics product for global change study. Remote Sens. Environ. 182, 13–26.

Gonsamo, A., Chen, J.M., Price, D.T., Kurz, W.A., Wu, C., 2012. Land surface phenology from optical satellite measurement and CO2 eddy covariance technique. J. Geophys. Res. Biogeosci. 117, 1472.

Graham, E.A., Riordan, E.C., Yuen, E.M., Estrin, D., Rundel, P.W., 2010. Public Internet-connected cameras used as a cross-continental ground-based plant phenology monitoring system. Glob. Chang. Biol. 16, 3014–3023.

Guan, K., Medvigy, D., Wood, E.F., Caylor, K.K., Li, S., Jeong, S., 2014. Deriving vegetation phenological time and trajectory information over Africa using SEVIRI daily LAI. IEEE Trans. Geosci. Remote Sens. 52, 1113–1130.

Guyon, D., Guillot, M., Vitasse, Y., Cardot, H., Hagolle, O., Delzon, S., Wigneron, J.P., 2011. Monitoring elevation variations in leaf phenology of deciduous broadleaf forests from SPOT/VEGETATION time-series. Remote Sens. Environ. 115, 615–627.

Guzman, J.P., Dash, J., Atkinson, P., 2018. Remote sensing of mangrove forest phenology and its environmental drivers. Remote Sens. Environ. 205, 71–84.

Hall-Beyer, M., 2003. Comparison of single-year and multiyear NDVI time series principal components in cold temperate biomes. IEEE Trans. Geosci. Remote Sens. 41, 2568–2574.

Han, Q., Wang, T., Jiang, Y., Fischer, R., Li, C., 2018. Phenological variation decreased carbon uptake in European forests during 1999–2013. For. Ecol. Manag. 427, 45–51.

Hanes, J.M., Schwartz, M.D., 2011. Modeling land surface phenology in a mixed temperate forest using MODIS measurements of leaf area index and land surface temperature. Theor. Appl. Climatol. 105, 37–50.

He, Y., Bo, Y., Jong, R.D., Li, A., Zhu, Y., Cheng, J., 2015. Comparison of vegetation phenological metrics extracted from GIMMS NDVIg and MERIS MTCI data sets over China. Int. J. Remote Sens. 36, 300–317.

Henebry, G.M., Beurs, K.M.D., 2013. Remote Sensing of Land Surface Phenology: A Prospectus.

Hermance, J.F., 2007. Stabilizing high-order, non-classical harmonic analysis of NDVI data for average annual models by damping model roughness. Int. J. Remote Sens. 28, 2801–2819.

Hermance, J.F., Jacob, R.W., Bradley, B.A., Mustard, J.F., 2007. Extracting phenological signals from multiyear AVHRR NDVI time series: framework for applying high-order annual splines with roughness damping. IEEE Trans. Geosci. Remote Sens. 45, 3264–3276.

Heumann, B.W., Seaquist, J.W., Eklundh, L., Jönsson, P., 2007. AVHRR derived phenological change in the Sahel and Soudan, Africa, 1982–2005. Remote Sens. Environ. 108, 385–392.

Hird, J.N., Mcdermid, G.J., 2009. Noise reduction of NDVI time series: an empirical comparison of selected techniques. Remote Sens. Environ. 113, 248–258.

Hodges, T., 1991. Temperature and Water Stress Effects on Phenology. pp. 7–13.

Hogda, K.A., Karlsen, S.R., Solheim, I., 2001. Climatic Change Impact on Growing Season in Fennoscandia Studied by a Time Series of NOAA AVHRR NDVI Data. pp. 1338–1340.

Holben, B., 1986. Characteristics of maximum-value composite images from temporal AVHRR data. Int. J. Remote Sens. 7, 1417–1434.

Hou, X., Gao, S., Zheng, N., Xu, Z., 2014. Extracting grassland vegetation phenology in North China based on cumulative SPOT-VEGETATION NDVI data. Int. J. Remote Sens. 35, 3316–3330.

Houborg, R., Mccabe, M.F., 2018. Daily retrieval of NDVI and LAI at 3 m resolution via the fusion of CubeSat, Landsat, and MODIS data. Remote Sens. 10, 890.

Huang, N.E., Shen, Z., Long, S.R., Wu, M.C., Shih, H.H., Zheng, Q., Yen, N.C., Chi, C.T., Liu, H.H., 1998. The empirical mode decomposition and the Hilbert spectrum for nonlinear and non-stationary time series analysis. Proc. Math. Phys. Eng. Sci. 454, 903–995.

Huete, A., 1988. A soil-adjusted vegetation index (SAVI). Remote Sens. Environ. 25, 295–309.

Huete, A., Justice, C., Leeuwen, W.V., 1999. MODIS Vegetation Index (MOD13). Algorithm Theoretical Basis Document.

Hufkens, K., Friedl, M., Sonnentag, O., Braswell, B.H., Milliman, T., Richardson, A.D., 2012. Linking near-surface and satellite remote sensing measurements of deciduous broadleaf forest phenology. Remote Sens. Environ. 117, 307–321.

Islam, A.S., Bala, S.K., 2008. Assessment of potato phenological characteristics using MODIS-derived NDVI and LAI information. Mapp. Sci. Remote Sens. 45, 454–470.

Jeong, S., Schimel, D., Frankenberg, C., Drewry, D.T., Fisher, J.B., Verma, M., Berry, J.A., Lee, J., Joiner, J., 2017. Application of satellite solar-induced chlorophyll fluorescence to understanding large-scale variations in vegetation phenology and function over northern high latitude forests. Remote Sens. Environ. 190, 178–187.

Ji, L., Brown, J.F., 2017. Effect of NOAA Satellite Orbital Drift on AVHRR-Derived Phenological Metrics. pp. 215–223.

Jia, K., Liang, S., Wei, X., Yao, Y., Su, Y., Jiang, B., Wang, X., 2014. Land cover classification of Landsat data with phenological features extracted from time series MODIS NDVI data. Remote Sens. 6, 11518–11532.

Jian, L., Roy, D.P., 2017. A global analysis of sentinel-2A, sentinel-2B and Landsat-8 data revisit intervals and implications for terrestrial monitoring. Remote Sens. 9, 902.

Jiang, Z., Huete, A.R., Didan, K., Miura, T., 2008. Development of a two-band enhanced vegetation index without a blue band. Remote Sens. Environ. 112, 3833–3845.

Jin, H., Eklundh, L., 2014. A physically based vegetation index for improved monitoring of plant phenology. Remote Sens. Environ. 152, 512–525.

Jin, Z., Xu, B., 2013. A novel compound smoother—RMMEH to reconstruct MODIS NDVI time series. IEEE Geosci. Remote Sens. Lett. 10, 942–946.

Jin, H., Jönsson, A.M., Bolmgren, K., Langvall, O., Eklundh, L., 2017. Disentangling remotely sensed plant phenology and snow seasonality at northern Europe using MODIS and the plant phenology index. Remote Sens. Environ. 198, 203–212.

Jones, J.W., Hoogenboom, G., Porter, C.H., Boote, K.J., Batchelor, W.D., Hunt, L.A., et al., 2003. The dssat cropping system model. Eur. J. Agron. 18 (3-4), 235–265.

Jones, M.O., Jones, L.A., Kimball, J.S., McDonald, K.C., 2011. Satellite passive microwave remote sensing for monitoring global land surface phenology. Remote Sens. Environ. 115, 1102–1114.

Jönsson, P., Eklundh, L., 2002. Seasonality extraction by function fitting to time-series of satellite sensor data. IEEE Trans. Geosci. Remote Sens. 40, 1824–1832.

Jönsson, P., Eklundh, L., 2004. TIMESAT—a program for analyzing time-series of satellite sensor data ☆. Comput. Geosci. 30, 833–845.

Jönsson, P., Cai, Z., Melaas, E., Friedl, M.A., Eklundh, L., 2018. A method for robust estimation of vegetation seasonality from Landsat and sentinel-2 time series data. Remote Sens. 10.

Julien, Y., Sobrino, J.A., 2010. Comparison of cloud-reconstruction methods for time series of composite NDVI data. Remote Sens. Environ. 114, 618–625.

Julitta, T., Cremonese, E., Migliavacca, M., Colombo, R., Galvagno, M., Siniscalco, C., Rossini, M., Fava, F., Cogliati, S., Cella, U.M.D., 2014. Using digital camera images to analyse snowmelt and phenology of a subalpine grassland. Agric. For. Meteorol. 198-199, 116–125.

Kandasamy, S., Baret, F., Verger, A., Neveux, P., 2013. A comparison of methods for smoothing and gap filling time series of remote sensing observations: application to MODIS LAI products. Biogeosciences 10(6), 4055–4071.

Kang, S., Running, S.W., Lim, J.H., Zhao, M., Park, C.R., Loehman, R., 2003. A regional phenology model for detecting onset of greenness in temperate mixed forests, Korea: an application of MODIS leaf area index. Remote Sens. Environ. 86, 232–242.

Kariyeva, J., Leeuwen, W.J.D.V., 2011. Environmental drivers of NDVI-based vegetation phenology in central Asia. Remote Sens. 3, 203–246.

Katharine, W., Jennifer, P., Paul, S., 2014. Remote sensing of spring phenology in northeastern forests: a comparison of methods, field metrics and sources of uncertainty. Remote Sens. Environ. 148, 97–107.

Keenan, T.F., Gray, J., Friedl, M.A., Toomey, M., Bohrer, G., Hollinger, D.Y., Munger, J.W., O Keefe, J., Schmid, H.P., Wing, I.S., 2014. Net carbon uptake has increased through warming-induced changes in temperate forest phenology. Nat. Clim. Chang. 4, 598–604.

Klosterman, S.T., Hufkens, K., Gray, J.M., Melaas, E., Sonnentag, O., Lavine, I., Mitchell, L., Norman, R., Friedl, M.A., Richardson, A.D., 2014a. Evaluating remote sensing of deciduous forest phenology at multiple spatial scales using PhenoCam imagery. Biogeosciences 11, 4305–4320.

Klosterman, S.T., Hufkens, K., Gray, J.M., Melaas, E., Sonnentag, O., Lavine, I., Mitchell, L., Norman, R., Friedl, M.A., Richardson, A.D., 2014b. Evaluating remote sensing of deciduous forest phenology at multiple spatial scales using PhenoCam imagery. Biogeosciences 11, 4305–4320.

Klosterman, S., Melaas, E., Wang, J., Martinez, A., Richardson, A.D., 2018. Fine-scale perspectives on landscape phenology from unmanned aerial vehicle (UAV) photography. Agric. For. Meteorol. 248, 397–407.

Kobayashi, H., Yunus, A.P., Nagai, S., Sugiura, K., Kim, Y., Dam, B.V., Nagano, H., Zona, D., Harazono, Y., Bret-Harte, M.S., 2016. Latitudinal gradient of spruce forest understory and tundra phenology in Alaska as observed from satellite and ground-based data. Remote Sens. Environ. 177, 160–170.

Li, J., Roy, D.P., 2017. A Global Analysis of Sentinel-2A, Sentinel-2B and Landsat-8 Data Revisit Intervals and Implications for Terrestrial Monitoring. GSCE Faculty Publications.

Li, X., Zhou, Y., Asrar, G.R., Mao, J., Li, X., Li, W., 2017. Response of vegetation phenology to urbanization in the conterminous United States. Glob. Chang. Biol. 23, 2818–2830.

Liang, L., Schwartz, M.D., Fei, S., 2011. Validating satellite phenology through intensive ground observation and landscape scaling in a mixed seasonal forest. Remote Sens. Environ. 115, 143–157.

Lieth, H., 1974. Purposes of a phenology book. In: Lieth, H. (Ed.), Phenology and Seasonality Modeling. Springer-Verlag, New York, pp. 3–19.

Lieth, H., Schwartz, M.D., 1997. In: Phenology in Seasonal Climates. Backhuys Publishers. Liu, L., Liang, L., Schwartz, M.D., Donnelly, A., Wang, Z., Schaaf, C.B., Liu, L., 2015. Evaluating the potential of MODIS satellite data to track temporal dynamics of autumn phenology in a temperate mixed forest. Remote Sens. Environ. 160, 156–165.

Liu, Y., Wu, C., Peng, D., Xu, S., Gonsamo, A., Jassal, R.S., Arain, M.A., Lu, L., Fang, B., Chen, J.M., 2016. Improved modeling of land surface phenology using MODIS land surface reflectance and

temperature at evergreen needleleaf forests of central North America. Remote Sens. Environ. 176, 152–162.

Liu, L., Zhang, X., Yu, Y., Guo, W., 2017. Real-time and short-term predictions of spring phenology in North America from VIIRS data. Remote Sens. Environ. 194, 89–99.

Liu, L., Cao, R., Shen, M., Chen, J., Wang, J., Zhang, X., 2019. How does scale effect influence spring vegetation phenology estimated from satellited-derived vegetation indexes? Remote sensing 11. https://doi.org/10.3390/rs11182137

Liu, Y., Hill, M.J., Zhang, X., Wang, Z., Richardson, A.D., Hufkens, K., Filippa, G., Baldocchi, D.D., Ma, S., Verfaillie, J., 2017. Using data from Landsat, MODIS, VIIRS and PhenoCams to monitor the phenology of California oak/grass savanna and open grassland across spatial scales. Agric. For. Meteorol. 237–238, 311–325.

Lloyd, D., 1990. A phenological classification of terrestrial vegetation cover using shortwave vegetation index imagery. Remote Sens. 11, 2269–2279.

Los, O.S., 1998. Estimation of the ratio of sensor degradation between NOAA AVHRR channels 1 and 2 from monthly NDVI composites. IEEE Trans. Geosci. Remote Sens. 36, 206–213.

Lovell, J.L., Graetz, R.D., 2001. Filtering pathfinder AVHRR land NDVI data for Australia. Int. J. Remote Sens. 22, 2649–2654.

Lu, L., Wang, C., Guo, H., Li, Q., 2014. Detecting winter wheat phenology with SPOTVEGETATION data in the North China Plain. Geocarto Int. 29, 244–255.

Ma, M., Veroustraete, F., 2006. Reconstructing pathfinder AVHRR land NDVI time-series data for the Northwest of China. Adv. Space Res. 37, 835–840.

Malik, A., Shakir, A.S., Ajmal, M., Khan, M.J., Khan, T.A., 2017. Assessment of AquaCrop model in simulating sugar beet canopy cover, biomass and root yield under different irrigation and field management practices in semi-arid regions of Pakistan. Water Resour. Manag. 1–18.

Martínez, B., Gilabert, M.A., 2009. Vegetation dynamics from NDVI time series analysis using the wavelet transform. Remote Sens. Environ. 113, 1823–1842.

Mayer, A., 2010. Phenology and citizen science. Bioscience 60, 172–175.

Mckellip, R.D., Ross, K.W., Spruce, J.P., Smoot, J.C., Ryan, R.E., Gasser, G.E., Prados, D.L., Vaughan, R.D., 2010. Phenological Parameters Estimation Tool. NASA Tech. Briefs, New York.

McMaster, G.S., White, J.W., Weiss, A., Baenziger, P.S., Wilhelm, W.W., Porter, J.R., Jamieson, P.D., 2008. Simulating Crop Phenological Responses to Water Deficits. American Society of Agronomy, Crop Science Society of America, Soil Science Society of America, Madison, WI, pp. 277–300.

Mcmaster, G.S., Wilhelm, W.W., 1997. Growing degree-days: one equation, two interpretations. Agricultural & Forest Meteorology 4(87), 291–300.

McNairn, H., Jiao, X., Pacheco, A., Sinha, A., Tan, W., Li, Y., 2018. Estimating canola phenology using synthetic aperture radar. Remote Sens. Environ. 219, 196–205.

Melaas, E.K., Friedl, M.A., Zhu, Z., 2013. Detecting interannual variation in deciduous broadleaf forest phenology using Landsat TM/ETM + data. Remote Sens. Environ. 132, 176–185.

Melaas, E.K., Sulla-Menashe, D., Gray, J.M., Black, T.A., Morin, T.H., Richardson, A.D., Friedl, M.A., 2016. Multisite analysis of land surface phenology in North American temperate and boreal deciduous forests from Landsat. Remote Sens. Environ. 186, 452–464.

Meroni, M., Fasbender, D., Kayitakire, F., Pini, G., Rembold, F., Urbano, F., Verstraete, M., 2013. Regional drought monitoring using phenologicallytuned biomass production estimates from SPOT-VEGETATION FAPAR. pp. 495–499.

Meroni, M., Verstraete, M.M., Rembold, F., Urbano, F., Kayitakire, F., 2014. A phenology-based method to derive biomass production anomalies for food security monitoring in the Horn of Africa. Int. J. Remote Sens. 35, 2472–2492.

Migliavacca, M., Galvagno, M., Cremonese, E., Rossini, M., Meroni, M., Sonnentag, O., Cogliati, S., Manca, G., Diotri, F., Busetto, L., 2011. Using digital repeat photography and eddy covariance data to model grassland phenology and photosynthetic CO_2 uptake. Agricultural & Forest Meteorology 10(151), 1325–1337.

Mobasheri, M.R., Chahardoli, M., Farajzadeh, M., 2010. Introducing PASAVI and PANDVI methods for sugarcane physiological date estimation, using ASTER images. J. Agric. Sci. Technol. A 12, 309–320.

Moody, A., Johnson, D.M., 2001. Land-surface phenologies from AVHRR using the discrete fourier transform. Remote Sens. Environ. 75, 305–323.

Moore, C.E., Brown, T., Keenan, T.F., Duursma, R.A., van Dijk, A.I.J.M., Beringer, J., Culvenor, D., Evans, B., Huete, A., Hutley, L.B., Maier, S., Restrepo-Coupe, N., Sonnentag, O., Specht, A., Taylor, J.R., van Gorsel, E., Liddell, M.J., 2016. Reviews and syntheses: Australian vegetation phenology digital repeat photography. Biogeosciences 13, 5085–5102.

Motohka, T., Nasahara, K.N., Oguma, H., Tsuchida, S., 2010. Applicability of green-red vegetation index for remote sensing of vegetation phenology. Remote Sens. 2, 2369–2387.

Moulin, S., Kergoat, L., Viovy, N., Dedieu, G., 1997. Global-scale assessment of vegetation phenology using NOAA/AVHRR satellite measurements. J. Clim. 10, 1154–1170.

Moura, Y.M.D., Galvão, L.S., Hilker, T., Jin, W., Saleska, S., Amaral, C.H.D., Nelson, B.W., Lopes, A.P., Wiedeman, K.K., Prohaska, N., 2017. Spectral analysis of amazon canopy phenology during the dry season using a tower hyperspectral camera and modis observations. ISPRS J. Photogrammetry Remote Sens. 131, 52–64.

Myneni, R.B.K.Y., 2003. User's Guide—FPAR, LAI 8-day composite NASA MODIS land algorithm. In: Terra MODIS Land Team.

Myneni, R.B., Keeling, C.D., Tucker, C.J., Asrar, G., Nemani, R.R., 1997. Increased plant growth in the northern high latitudes from 1981 to 1991. Nature 386, 698–702.

Nagol, J., Vermote, E., Prince, S., 2014. Quantification of impact of orbital drift on interannual trends in AVHRR NDVI data. Remote Sens. 6, 6680–6687.

Nasahara, K.N., Nagai, S., 2015. Review: development of an in situ observation network for terrestrial ecological remote sensing: the Phenological Eyes Network (PEN). Ecol. Res. 30, 211–223.

Nemani, R., Hashimoto, H., Votava, P., Melton, F., Wang, W.L., Michaelis, A., Mutch, L., Milesi, C., Hiatt, S., White, M., 2009. Monitoring and forecasting ecosystem dynamics using the terrestrial observation and prediction system (TOPS). Remote Sens. Environ. 113, 1497–1509.

Nijland, W., Bolton, D.K., Coops, N.C., Stenhouse, G., 2016. Imaging phenology; scaling from camera plots to landscapes. Remote Sens. Environ. 177, 13–20.

Onojeghuo, A.O., Blackburn, G.A., Wang, Q., Atkinson, P.M., Kindred, D., Miao, Y., 2018. Rice crop phenology mapping at high spatial and temporal resolution using downscaled MODIS time-series. GIScience Remote Sens.

Pan, Z., Huang, J., Zhou, Q., Wang, L., Cheng, Y., Zhang, H., Blackburn, G.A., Yan, J., Liu, J., 2015. Mapping crop phenology using NDVI time-series derived from HJ-1 A/B data. Int. J. Appl. Earth Obs. Geoinf. 34, 188–197.

Park, J., Tateishi, R., Matsuoka, M., 1999. A proposal of the Temporal Window Operation (TWO) method to remove high-frequency noises in AVHRR NDVI time series data. Journal of the Japan Society of Photogrammetry and Remote Sensing 38 (5), 36–47. https://doi.org/10.4287/jsprs.38.5_36

Pastick, N.J., Wylie, B.K., Wu, Z., 2018. Spatiotemporal Analysis of Landsat-8 and Sentinel-2 Data to Support Monitoring of Dryland Ecosystems. Remote sensing 10 (5). https://doi.org/10.3390/rs10050791

Peltoniemi, M., Aurela, M., Böttcher, K., Kolari, P., Loehr, J., Hokkanen, T., Karhu, J., Linkosalmi, M., Tanis, C.M., Metsämäki, S., 2018. Networked web-cameras monitor congruent seasonal development of birches with phenological field observations. Agric. For. Meteorol. 249, 335–347.

Peng, D., Zhang, X., Zhang, B., Liu, L., Liu, X., Huete, A.R., Huang, W., Wang, S., Luo, S., Zhang, X., 2017. Scaling effects on spring phenology detections from MODIS data at multiple spatial resolutions over the contiguous United States. ISPRS J. Photogrammetry Remote Sens. 132, 185–198.

Peng, D., Wu, C., Zhang, X., Le, Y., Huete, A.R., Wang, F., Luo, S., Liu, X., Zhang, H., 2018. Scaling up spring phenology derived from remote sensing images. Agric. For. Meteorol. 256–257, 207–219.

Reed, B.C., Brown, J.F., VanderZee, D., Loveland, T.R., Merchant, J.W., Ohlen, D.O., 1994. Measuring phenological variability from satellite imagery. J. Veg. Sci. 5, 703–714.

Richardson, A.D., Jenkins, J.P., Braswel, B.H., Hollinger, D.Y., Ollinger, S.V., Smith, M.L., 2007. Use of digital webcam images to track spring green-up in a deciduous broadleaf forest. Oecologia 2 (152), 323–334.

Richardson, A.J., Wiegand, C.L., 1978. Distinguishing Vegetation from Soil Background Information. Richardson, A., A. Friedl, M., Frolking, S., Pless, R., Collaborators, P., 2011. PhenoCam: a continental-scale observatory for monitoring the phenology of terrestrial vegetation. Am. Geophys. Union, Fall Meet. 517.

Richardson, A.D., Hufkens, K., Milliman, T., Frolking, S., 2018. Intercomparison of phenological transition dates derived from the PhenoCam Dataset V1.0 and MODIS satellite remote sensing. Sci. Rep. 8, 5679.

Rodrigues, A., Marcal, A.R.S., Cunha, M., 2012. Phenology Parameter Extraction from Time-Series of Satellite Vegetation Index Data Using Phenosat. pp. 4926–4929.

Rodrigues, A., Marcal, A.R.S., Cunha, M., 2013. Monitoring vegetation dynamics inferred by satellite data using the PhenoSat tool. IEEE Trans. Geosci. Remote Sens. 51, 2096–2104.

Roerink, G.J., Menenti, M., Verhoef, W., 2000. Reconstructing cloudfree NDVI composites using Fourier analysis of time series. Int. J. Remote Sens. 21, 1911–1917.

Rouse, J.W., 1973. Monitoring Vegetation Systems in the Great Plains with ERTS. vol. 1. Third ERTS Symposium, NASA, Washington, DC, pp. 309–317.

Sakamoto, T., 2018a. Refined shape model fitting methods for detecting various types of phenological information on major U.S. crops. ISPRS J. Photogrammetry Remote Sens. 138, 176–192.

Sakamoto, T., 2018b. Refined shape model fitting methods for detecting various types of phenological information on major U.S. crops. ISPRS J. Photogrammetry Remote Sens. 138, 176–192.

Sakamoto, T., Yokozawa, M., Toritani, H., Shibayama, M., Ishitsuka, N., Ohno, H., 2005. A crop phenology detection method using time-series MODIS data. Remote Sens. Environ. 96, 366–374.

Sakamoto, T., Wardlow, B.D., Gitelson, A.A., Verma, S.B., Suyker, A.E., Arkebauer, T.J., 2010. A Two-Step Filtering approach for detecting maize and soybean phenology with time-series MODIS data. Remote Sens. Environ. 114, 2146–2159.

Sakamoto, T., Gitelson, A.A., Arkebauer, T.J., 2013. MODIS-based corn grain yield estimation model incorporating crop phenology information. Remote Sens. Environ. 131, 215–231.

Sellers, P.J., Tucker, C.J., Collatz, G.J., Los, S.O., Justice, C.O., Dazlich, D.A., Randall, D.A., 1994. A global 1° by 1° NDVI data set for climate studies. Part 2: the generation of global fields of terrestrial biophysical parameters from the NDVI. Int. J. Remote Sens. 15, 3519–3545.

Shabanov, N.V., Zhou, L., Knyazikhin, Y., Myneni, R.B., 2002. Analysis of interannual changes in northern vegetation activity observed in AVHRR data from 1981 to 1994. IEEE Transactions on Geoscience & Remote Sensing 1(40), 115–130.

Shen, M., Tang, Y., Chen, J., Zhu, X., Zheng, Y., 2011. Influences of temperature and precipitation before the growing season on spring phenology in grasslands of the central and eastern Qinghai-Tibetan Plateau. Agric. For. Meteorol. 151, 1711–1722.

Sonnentag, O., Hufkens, K., Teshera-Sterne, C., Young, A.M., Friedl, M., Braswell, B.H., Milliman, T., O Keefe, J., Richardson, A.D., 2012. Digital repeat photography for phenological research in forest ecosystems. Agric. For. Meteorol. 152, 159–177.

Sun, L., Gao, F., Anderson, M.C., Kustas, W.P., Thenkabail, P.S., 2017. Remote sensing daily mapping of 30 m LAI and NDVI for grape yield prediction in California vineyards. Remote Sens. 9, 317.

Tan, B., Morisette, J.T., Wolfe, R.E., Gao, F., Ederer, G.A., Nightingale, J., Pedelty, J.A., 2011. An enhanced TIMESAT algorithm for estimating vegetation phenology metrics from MODIS data. IEEE J. Sel. Top. Appl. Earth Observ. Remote Sens. 4, 361–371.

Tateishi, R., Ebata, M., 2004. Analysis of phenological change patterns using 1982–2000 advanced very high resolution radiometer (AVHRR) data. Int. J. Remote Sens. 25, 2287–2300.

Templ, B., Koch, E., Bolmgren, K., Ungersb Ck, M., Paul, A., Scheifinger, H., Rutishauser, T., Busto, M., Chmielewski, F., Hájková, L., 2018. Pan European Phenological database (PEP725): a single point of access for European data. Int. J. Biometeorol. 62, 1–5.

Thompson, D.R., Wehmanen, O.A., 1979. Using Landsat digital data to detect moisture stress. Photogramm. Eng. Remote Sens. 45, 201–207.

Thorpe, A.S., Barnett, D.T., Elmendorf, S.C., Hinckley, E.S., Hoekman, D., Jones, K.D., LeVan, K.E., Meier, C.L., Stanish, L.F., Thibault, K.M., 2016. Introduction to the sampling designs of the national ecological observatory network terrestrial observation system. Ecosphere 7, e1627.

Tian, F., Fensholt, R., Verbesselt, J., Grogan, K., Horion, S., Wang, Y., 2015. Evaluating temporal consistency of long-term global NDVI datasets for trend analysis. Remote Sens. Environ. 163, 326–340.

Tong, X., Tian, F., Brandt, M., Liu, Y., Zhang, W., Fensholt, R., 2019. Trends of land surface phenology derived from passive microwave and optical remote sensing systems and associated drivers across the dry tropics 1992–2012. Remote Sens. Environ. 232, 111307.

Townshend, J., Justice, C., Li, W., Gurney, C., Mcmanus, J., 1991. Global land cover classification by remote sensing: present capabilities and future possibilities. Remote Sens. Environ. 35, 243–255.

Tucker, C.J., 1979. Red and photographic infrared linear combinations for monitoring vegetation. Remote Sens. Environ. 8, 127–150.

Udelhoven, T., 2011. TimeStats: a software tool for the retrieval of temporal patterns from global satellite archives. IEEE J. Sel. Top. Appl. Earth Observ. Remote Sens. 4, 310–317.

van Leeuwen, W.J.D., Orr, B.J., Marsh, S.E., Herrmann, S.M., 2006. Multi-sensor NDVI data continuity: uncertainties and implications for vegetation monitoring applications. Remote Sens. Environ. 100, 67–81.

Verger, A., Baret, F., Weiss, M., 2011. A multisensor fusion approach to improve LAI time series. Remote Sens. Environ. 115, 2460–2470.

Verhegghen, A., Bontemps, S., Defourny, P., 2014. A global NDVI and EVI reference data set for land-surface phenology using 13 years of daily SPOT-VEGETATION observations. Int. J. Remote Sens. 35, 2440–2471.

Verstraete, M.M., Gobron, N., Aussedat, O., Robustelli, M., Pinty, B., Widlowski, J.L., Taberner, M., 2008. An automatic procedure to identify key vegetation phenology events using the JRC-FAPAR products. Adv. Space Res. 41, 1773–1783.

Viña, A., Gitelson, A.A., Rundquist, D.C., Keydan, G., Leavitt, B., Schepers, J., 2004. Monitoring maize (*Zea mays* L.) phenology with remote sensing. Agron. J. 2, 2729–2747.

Vintrou, E., Bégué, A., Baron, C., Saad, A., Lo Seen, D., Traoré, S., 2014. A Comparative Study on Satellite- and Model-Based Crop Phenology in West Africa. Remote Sensing 6(2), 1367–1389. https://doi.org/10.3390/rs6021367.

Viovy, N., Arino, O., Belward, A.S., 1992. The Best Index Slope Extraction (BISE): a method for reducing noise in NDVI time-series. Int. J. Remote Sens. 13, 1585–1590.

Vliet, A.J.H.V., de Groot, R.S., Bellens, Y., Braun, P., Bruegger, R., Bruns, E., Clevers, J., Estreguil, C., Flechsig, M., Jeanneret, F.O., 2003. The European Phenology Network.

Vrieling, A., Leeuw, J.D., Said, M.Y., 2013. Length of growing period over Africa: variability and trends from 30 Years of NDVI time series. Remote Sens. 5, 982–1000.

Vrieling, A., Skidmore, A.K., Wang, T., Meroni, M., Paganini, M., 2017. Spatially detailed retrievals of spring phenology from single-season high-resolution image time series. Int. J. Appl. Earth Obs. Geoinf. 59, 19–30.

Vrieling, A., Meroni, M., Darvishzadeh, R., Skidmore, A.K., Wang, T., Zurita-Milla, R., Oosterbeek, K., O'Connor, B., Paganini, M., 2018. Vegetation phenology from Sentinel-2 and field cameras for a Dutch barrier island. Remote Sens. Environ.

Wagenseil, H., Samimi, C., 2006a. Assessing spatio-temporal variations in plant phenology using Fourier analysis on NDVI time series: results from a dry savannah environment in Namibia. Int. J. Remote Sens. 27, 3455–3471.

Wagenseil, H., Samimi, C., 2006b. Assessing spatio-temporal variations in plant phenology using Fourier analysis on NDVI time series: results from a dry savannah environment in Namibia. Int. J. Remote Sens. 27, 3455–3471.

Walker, J.J., de Beurs, K.M., Wynne, R.H., 2014. Dryland vegetation phenology across an elevation gradient in Arizona, USA, investigated with fused MODIS and Landsat data. Remote Sens. Environ. 144, 85–97.

Walker, J.J., de Beurs, K.M., Wynne, R.H., Gao, F., 2012. Evaluation of Landsat and MODIS data fusion products for analysis of dryland forest phenology. Remote Sens. Environ. 117, 381–393.

Walther, S., Voigt, M., Thum, T., Gonsamo, A., Zhang, Y., Köhler, P., Jung, M., Varlagin, A., Guanter, L., 2015. Satellite chlorophyll fluorescence measurements reveal largescale decoupling of photosynthesis and greenness dynamics in boreal evergreen forests. Glob. Chang. Biol. 22.

Wang, D., Morton, D., Masek, J., Wu, A., Nagol, J., Xiong, X., Levy, R., Vermote, E., Wolfe, R., 2012. Impact of sensor degradation on the MODIS NDVI time series. Remote Sens. Environ. 119, 55–61.

Wang, C., Hunt, E.R., Zhang, L., Guo, H., 2013. Phenology-assisted classification of C-3 and C-4 grasses in the US Great Plains and their climate dependency with MODIS time series. Remote Sens. Environ. 138, 90–101.

Wang, J., Huang, J., Wang, X., Jin, M., Zhou, Z., Guo, Q., Zhao, Z., Huang, W., Zhang, Y., Song, X., 2015. Estimation of rice phenology date using integrated HJ-1 CCD and Landsat-8 OLI vegetation indices time-series images. J. Zhejiang Univ.—Sci. B 16, 832–844.

Wang, C., Li, J., Liu, Q., Zhong, B., Wu, S., Xia, C., 2017. Analysis of differences in phenology extracted from the enhanced vegetation index and the leaf area index. Sensors 17, 1982.

Wardlow, B.D., Egbert, S.L., 2008. Large-area crop mapping using time-series MODIS 250m NDVI data: an assessment for the U.S. Central Great Plains. Remote Sens. Environ. 112, 1096–1116.

Wardlow, B.D., Kastens, J.H., Egbert, S.L., 2006. Using USDA crop progress data for the evaluation of greenup onset date calculated from MODIS 250-meter data. Photogram. Eng. Remote Sens. 72, 1225–1234.

Watson, D.J., 1947. Comparative physiological studies on the growth of field crops: I. Variation in net assimilation rate and leaf area between species and varieties, and within and between years. Ann. Botany 11, 41–76.

White, M.A., Nemani, R.R., 2006. Real-time monitoring and short-term forecasting of land surface phenology. Remote Sens. Environ. 104, 43–49.

White, M.A., Thornton, P.E., Running, S.W., 1997. A continental phenology model for monitoring vegetation responses to interannual climatic variability. Glob. Biogeochem. Cycles 11, 217–234.

White, M.A., De Beurs, K.M., Didan, K., Inouye, D.W., Richardson, A.D., Jensen, O.P., O'Keefe, J., Zhang, G., Nemani, R.R., Van Leeuwen, W.J.D., 2009. Intercomparison, interpretation, and assessment of spring phenology in North America estimated from remote sensing for 1982–2006. Glob. Change Biol. 15, 613–615.

White, K., Pontius, J., Schaberg, P., 2014. Remote sensing of spring phenology in northeastern forests: a comparison of methods, field metrics and sources of uncertainty. Remote Sens. Environ. 148, 97–107.

Wingate, L., Ogée, J., Cremonese, E., Filippa, G., Mizunuma, T., Migliavacca, M., Moisy, C., Wilkinson, M., Moureaux, C., Wohlfahrt, G., 2015. Interpreting canopy development and physiology using a European phenology camera network at flux sites. Biogeosciences 12 (20), 7979–8034.

Wu, A., 1993. A method for determing the sensor degradation rates of NOAA AVHRR channels 1 and 2. Q. J. Appl. Meteorol. 33, 118–128.

Wu, C., Chen, J., Black, A., Price, D., Kurz, W., Desai, A., Gonsamo, A., Jassal, R., 2013. Interannual variability of net ecosystem productivity in forests is explained by carbon flux phenology in autumn. Global Ecology and Biogeography 22(8), 994–1006. https://doi.org/10.1111/geb.12044

Wu, C., Gonsamo, A., Gough, C.M., Chen, J.M., Xu, S., 2014. Modeling growing season phenology in North American forests using seasonal mean vegetation indices from MODIS. Remote Sens. Environ. 147, 79–88.

Wu, C., Hou, X., Peng, D., Gonsamo, A., Xu, S., 2016. Land surface phenology of China's temperate ecosystems over 1999–2013: spatial–temporal patterns, interaction effects, covariation with climate and implications for productivity. Agric. For. Meteorol. 216, 177–187.

Wu, C., Peng, D., Soudani, K., Siebicke, L., Gough, C.M., Arain, M.A., Bohrer, G., Lafleur, P.M., Peichl, M., Gonsamo, A., 2017. Land surface phenology derived from normalized difference vegetation index (NDVI) at global FLUXNET sites. Agric. For. Meteorol. 233, 171–182.

Wulder, M.A., Loveland, T.R., Roy, D.P., Crawford, C.J., Masek, J.G., Woodcock, C.E., Allen, R.G., Anderson, M.C., Belward, A.S., Cohen, W.B., Dwyer, J., Erb, A., Gao, F., Griffiths, P., Helder, D., Hermosilla, T., Hipple, J.D., Hostert, P., Hughes, M.J., Huntington, J., Johnson, D.M., Kennedy, R., Kilic, A., Li, Z., Lymburner, L., McCorkel, J., Pahlevan, N., Scambos, T.A., Schaaf, C., Schott, J.R., Sheng, Y., Storey, J., Vermote, E., Vogelmann, J., White, J.C., Wynne, R.H., Zhu, Z., 2019. Current status of Landsat program, science, and applications. Remote Sens. Environ. 225, 127–147.

Xu, X., Conrad, C., Doktor, D., 2017. Optimising phenological metrics extraction for different crop types in Germany using the moderate resolution imaging spectrometer (MODIS). Remote Sens. 9, 254.

Xue, Z., Du, P., Feng, L., 2014. Phenology-driven land cover classification and trend analysis based on long-term remote sensing image series. IEEE J. Select. Top. Appl. Earth Observ. Remote Sens. 7, 1142–1156.

Yan, D., Zhang, X., Yu, Y., Guo, W., Hanan, N.P., 2016a. Characterizing land surface phenology and responses to rainfall in the Sahara Desert. J. Geophys. Res. 121.

Yan, D., Zhang, X., Yu, Y., Guo, W., 2016b. A comparison of tropical rainforest phenology retrieved from geostationary (SEVIRI) and polar-orbiting (MODIS) sensors across the Congo basin. IEEE Trans. Geosci. Remote Sens. 54, 4867–4881.

Yang, Z., Shao, Y., Li, K., Liu, Q., Liu, L., Brian, B., 2017. An improved scheme for rice phenology estimation based on time-series multispectral HJ-1A/B and polarimetric RADARSAT-2 data. Remote Sensing of Environment 195, 184–201. https://doi.org/ 10.1016/j.rse.2017.04.016

Yang, Z., Wu, B., Zhang, M., Zeng, H., 2016. Crop phenology detection using high spatiotemporal resolution data fused from SPOT5 and MODIS products. Sensors 16, 2099.

Yu, F., Price, K.P., Ellis, J., Shi, P., 2003. Response of seasonal vegetation development to climatic variations in eastern central Asia. Remote Sens. Environ. 87, 42–54.

Zeng, L., Wardlow, B.D., Wang, R., Shan, J., Tadesse, T., Hayes, M.J., Li, D., 2016. A hybrid approach for detecting corn and soybean phenology with time-series MODIS data. Remote Sens. Environ. 181, 237–250.

Zhang, X., 2015. Reconstruction of a complete global time series of daily vegetation index trajectory from long-term AVHRR data. Remote Sens. Environ. 156, 457–472.

Zhang, X., Goldberg, M.D., 2011. Monitoring fall foliage coloration dynamics using time-series satellite data. Remote Sens. Environ. 115, 382–391.

Zhang, G.P., Qi, M., 2005. Neural network forecasting for seasonal and trend time series. Eur. J. Oper. Res. 160, 501–514.

Zhang, X., Friedl, M.A., Schaaf, C.B., Strahler, A.H., Hodges, J.C.F., Gao, F., Reed, B.C., Huete, A., 2003. Monitoring vegetation phenology using MODIS time-series data. Remote Sens. Environ. 84, 471–475.

Zhang, X., Friedl, M.A., Schaaf, C.B., 2006. Global vegetation phenology from Moderate Resolution Imaging Spectroradiometer (MODIS): evaluation of global patterns and comparison with in situ measurements. J. Geophys. Res. Biogeosci. 111, 367–375.

Zhang, X., Friedl, M.A., Schaaf, C.B., 2009. Sensitivity of vegetation phenology detection to the temporal resolution of satellite data. Int. J. Remote Sens. 30, 2061–2074.

Zhang, X., Goldberg, M.D., Yu, Y., 2012. Prototype for monitoring and forecasting fall foliage coloration in real time from satellite data. Agric. For. Meteorol. 158-159, 21–29.

Zhang, X., Wang, J., Gao, F., Liu, Y., Schaaf, C., Friedl, M., Yu, Y., Jayavelu, S., Gray, J., Liu, L., 2017b. Exploration of scaling effects on coarse resolution land surface phenology. Remote Sens. Environ. 190, 318–330.

Zhang, Y., Song, C., Band, L.E., Sun, G., Li, J., 2017c. Reanalysis of global terrestrial vegetation trends from MODIS products: browning or greening? Remote Sens. Environ. 191, 145–155.

Zhang, X., Jayavelu, S., Liu, L., Friedl, M.A., Henebry, G.M., Liu, Y., Schaaf, C.B., Richardson, A.D., Gray, J., 2018a. Evaluation of land surface phenology from VIIRS data using time series of PhenoCam imagery. Agric. For. Meteorol. 256-257, 137–149.

Zhang, X., Liu, L., Liu, Y., Senthilnath, J., Wang, J., Moon, M., Henebry, G.M., Friedl, M.A., Schaaf, C., 2018b. Generation and evaluation of the VIIRS land surface phenology product. Remote Sens. Environ. 216.

Zhao, H., Yang, Z., Di, L., Pei, Z., 2011. Evaluation of Temporal Resolution Effect in Remote Sensing Based Crop Phenology Detection Studies. pp. 135–150.

Zheng, Y., Wu, B., Zhang, M., Zeng, H., 2016. Crop phenology detection using high spatiotemporal resolution data fused from SPOT5 and MODIS products. Sensors 16, 2099.

Zhou, J., Jia, L., Menenti, M., 2015. Reconstruction of global MODIS NDVI time series: performance of harmonic ANalysis of time series (HANTS). Remote Sens. Environ. 163, 217–228.

Zhou, Q., Rover, J., Brown, J., Worstell, B., Howard, D., Wu, Z., Gallant, A.L., Rundquist, B., Burke, M., 2019. Monitoring landscape dynamics in central U.S. Grasslands with harmonized Landsat-8 and sentinel-2 time series data. Remote Sensing 11.

Zhu, X., Chen, J., Gao, F., Chen, X., Masek, J.G., 2010. An enhanced spatial and temporal adaptive reflectance fusion model for complex heterogeneous regions. Remote Sens. Environ. 114, 2610–2623.

Zhu, W., Pan, Y., He, H., Wang, L., Mou, M., Liu, J., 2012. A changing-weight filter method for reconstructing a high-quality NDVI time series to preserve the integrity of vegetation phenology. IEEE Trans. Geosci. Remote Sens. 50, 1085–1094.